Using electron backscatter diffraction (EBSD) to understand microstructure in mineral deposits

Alan Boyle

UNIVERSITY OF LIVERPOOL


2 cm

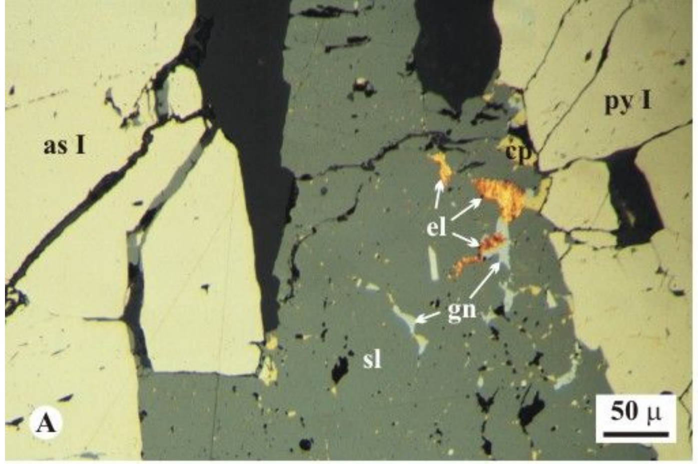
as I
py I
cp
el
gn
sl
A
50 µ

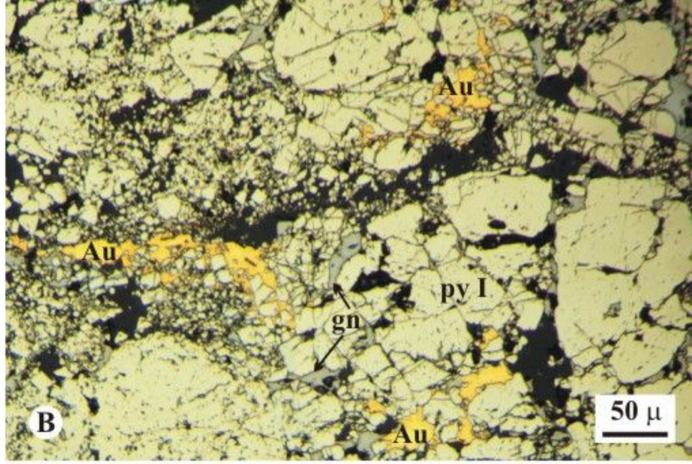
Au
Au
py I
gn
B
Au
50 µ

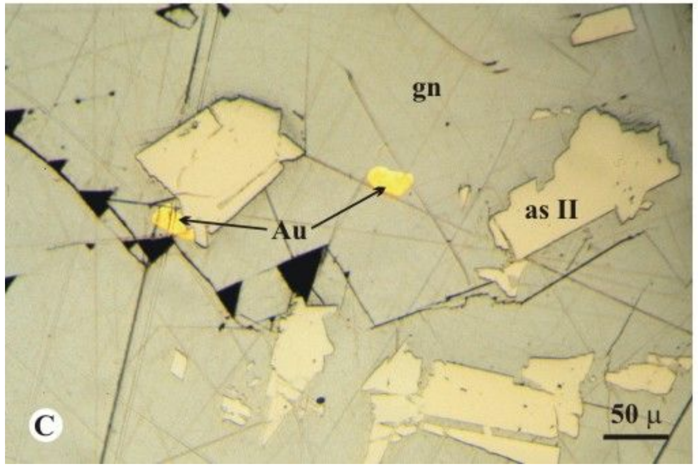
gn
Au
as II
C
50 µ

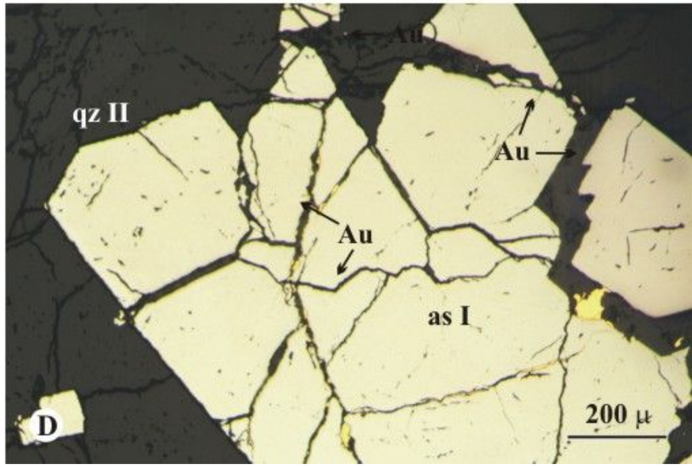
Au
qz II
Au
Au
as I
D
200 µ

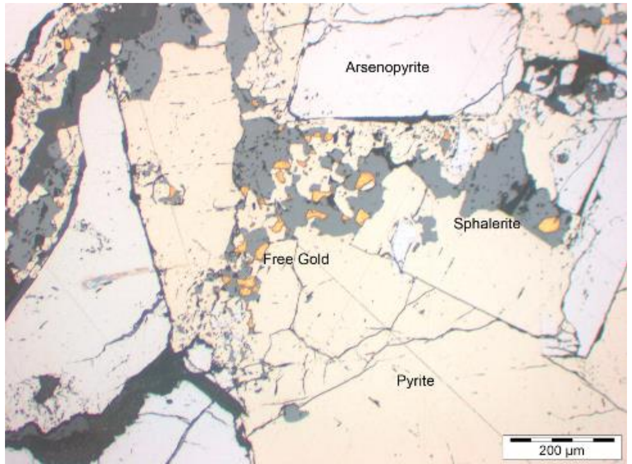
Arsenopyrite
Sphalerite
Free Gold
Pyrite
200 µm

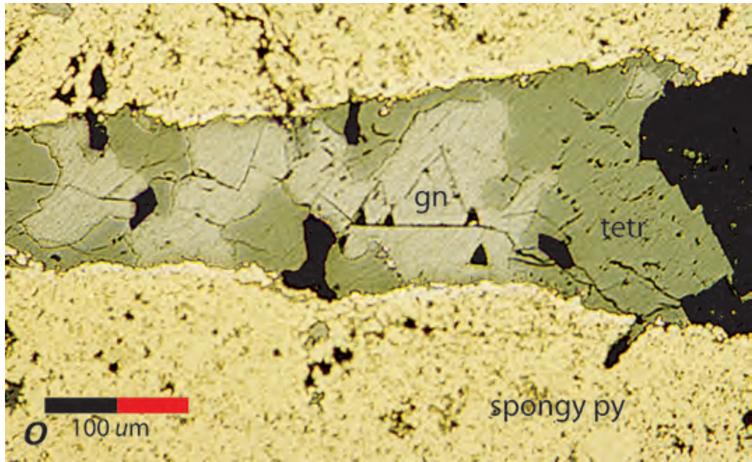
gn
tetr
spongy py
100 um

Structure of talk

- What is EBSD?
- Implications: Interpretation of some common textures
- Implications: Sphalerite colloform growth
- Implications: Quantifying pyrite deformation microstructure in experimentally and naturally deformed ores.
- Implications: Application to SAFOD
- Implications: The future - combine EBSD and microchemistry - invisible/visible gold

Specimen-Beam Interactions

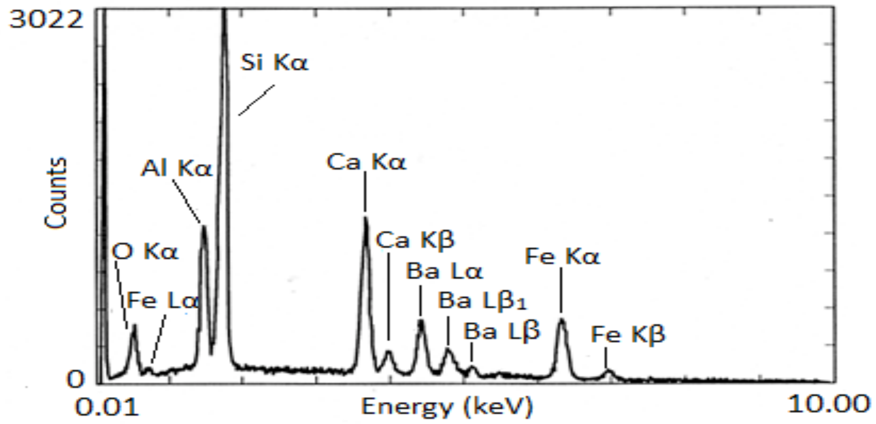

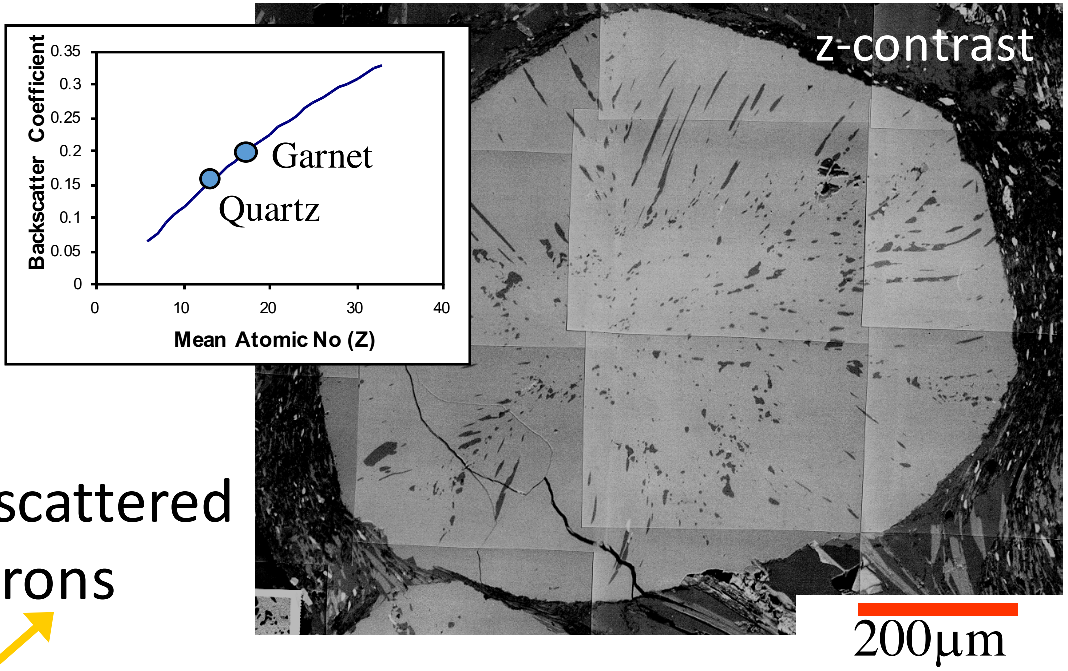

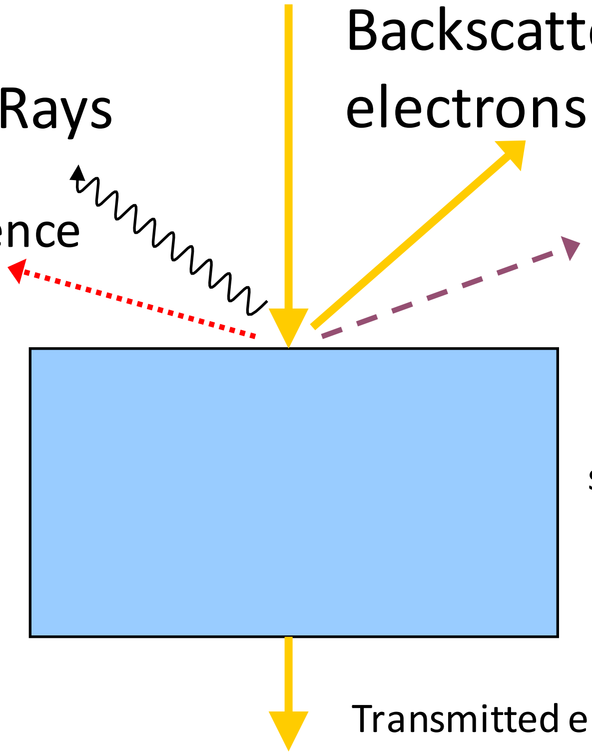

Used in SEM

Quartz grains in Triassic Paris Basin

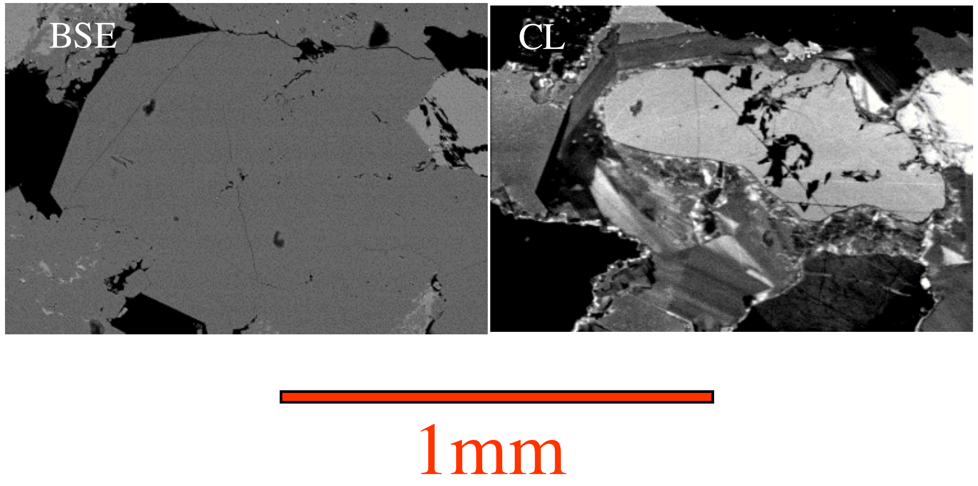

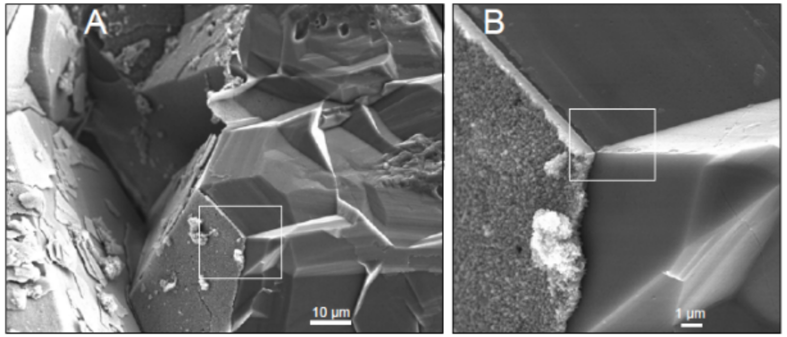

Worden et al. (2012, Geology)

Camscan X500 Crystal probe SEM

Orientation contrast (OC) image

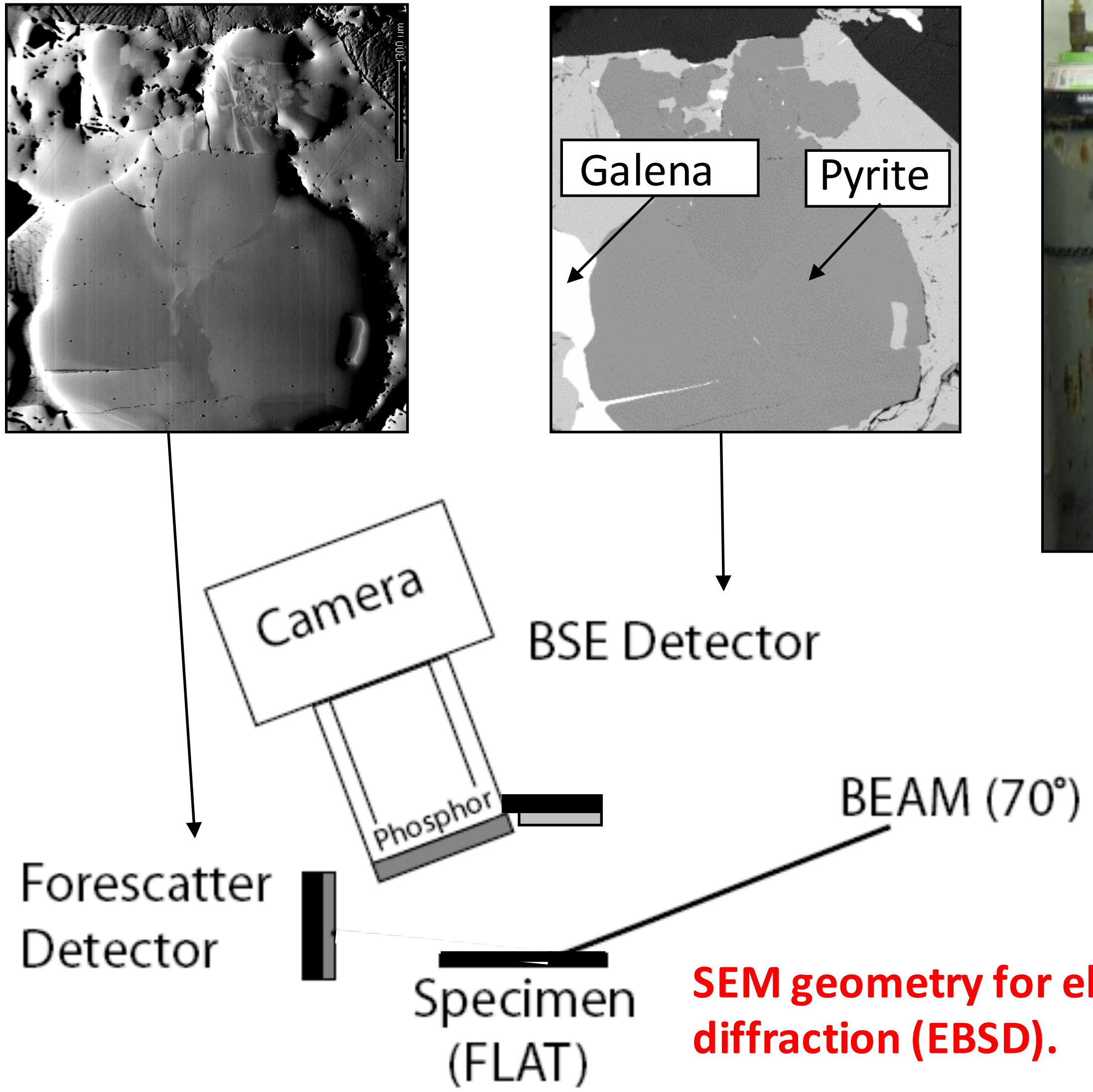

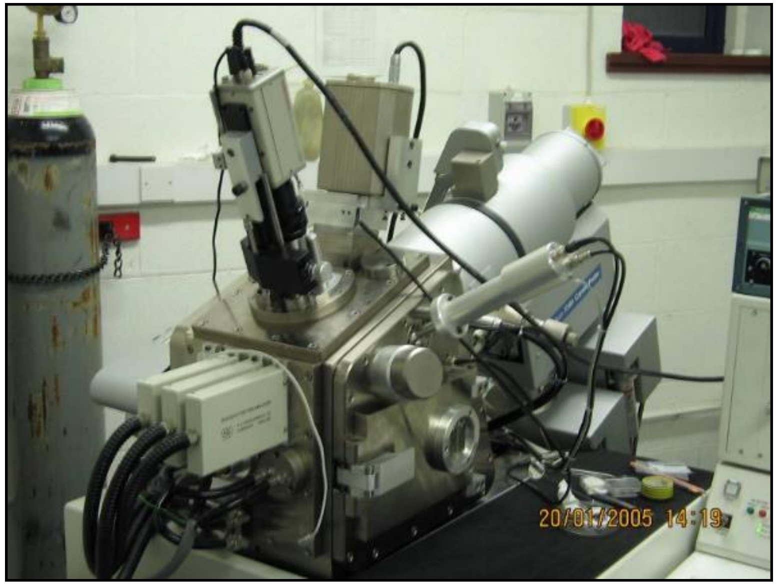

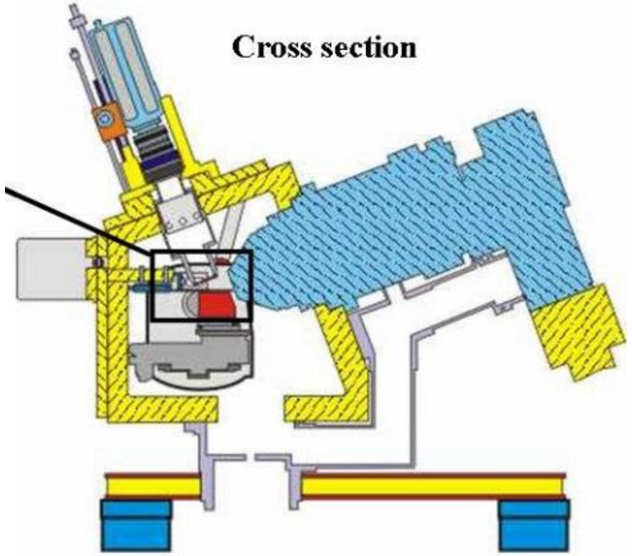

SEM geometry for electron backscatter diffraction (EBSD).

Gun is tilted at 70° to vertical.

Fig. 3.11.
a Lattice with two types of point defects. **b** Edge dislocation defined by the edge of a half-plane in a distorted crystal lattice. **c** Screw dislocation defined by a twisted lattice. **d** Dislocation with edge and screw dislocation regions in a crystal. A square itinerary of *closed arrows* around the dislocation is used to find the Burgers vector of the dislocation, indicated by *open arrows*

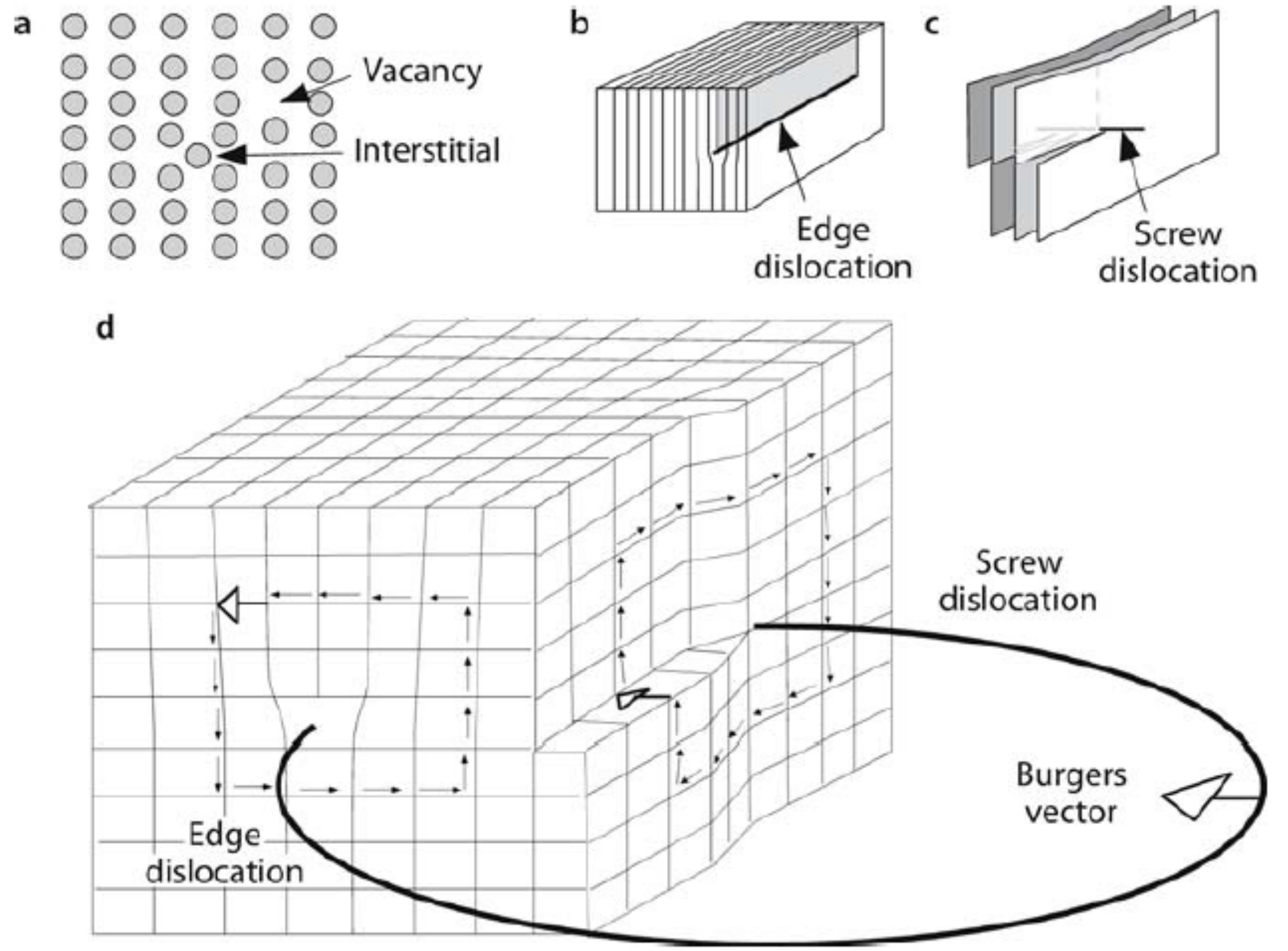

From Passchier & Trouw (2005)

r
ke

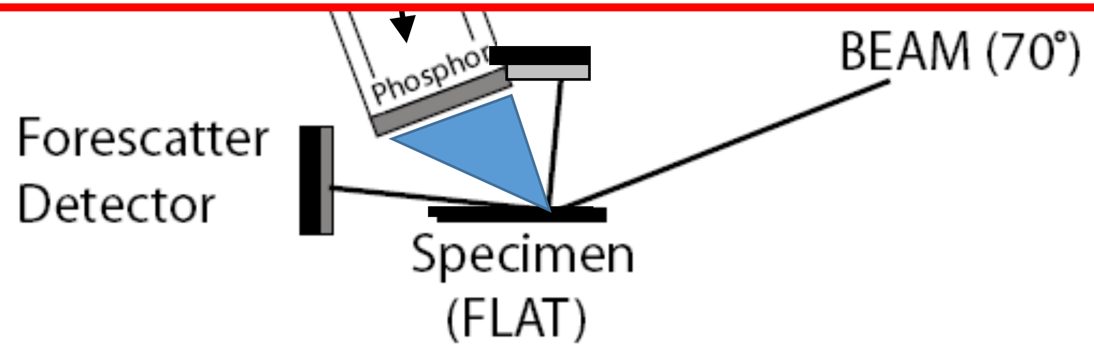

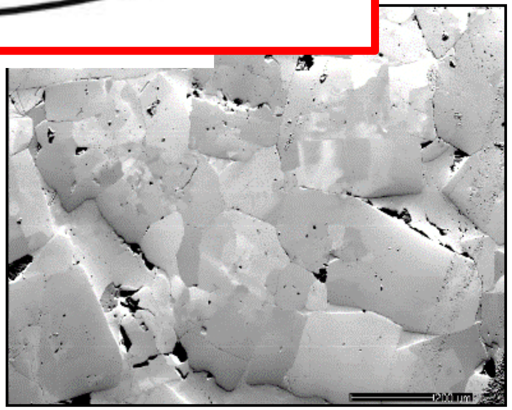

Euler-angle map

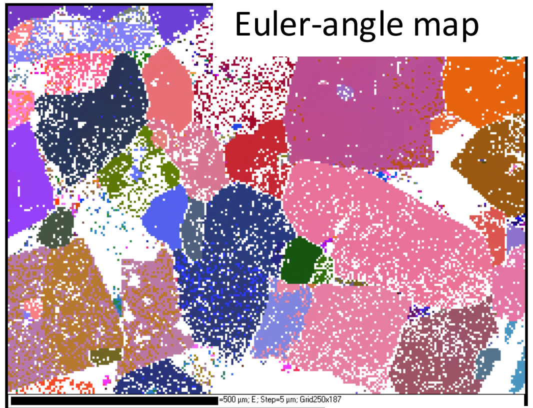

BC image

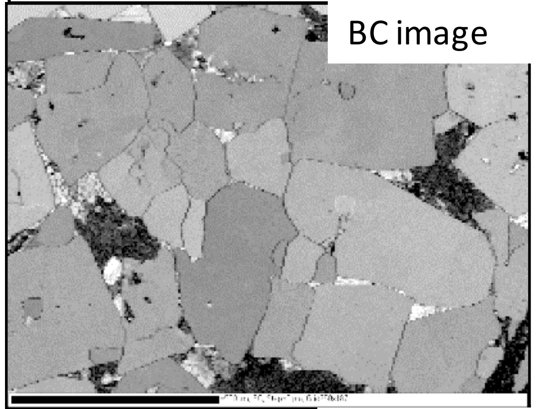

Processed

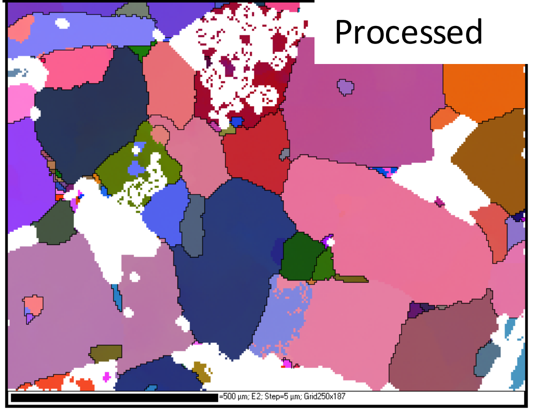

Secondary metamorphic recrystallisation textures in pyrite

Aim to show how EBSD can change interpretation of:

Foam/annealing Textures

Replacement Textures

Foam Textures in pyrite

- Evidence of “textural equilibrium” through high temperature annealing.
- Previous textures and accumulated dislocations are lost.
- Primarily identified through appearance of triple junctions in reflected light and BSE images.
- Numerous studies suggested that foam textures predominate above 500 °C and brittle textures below.

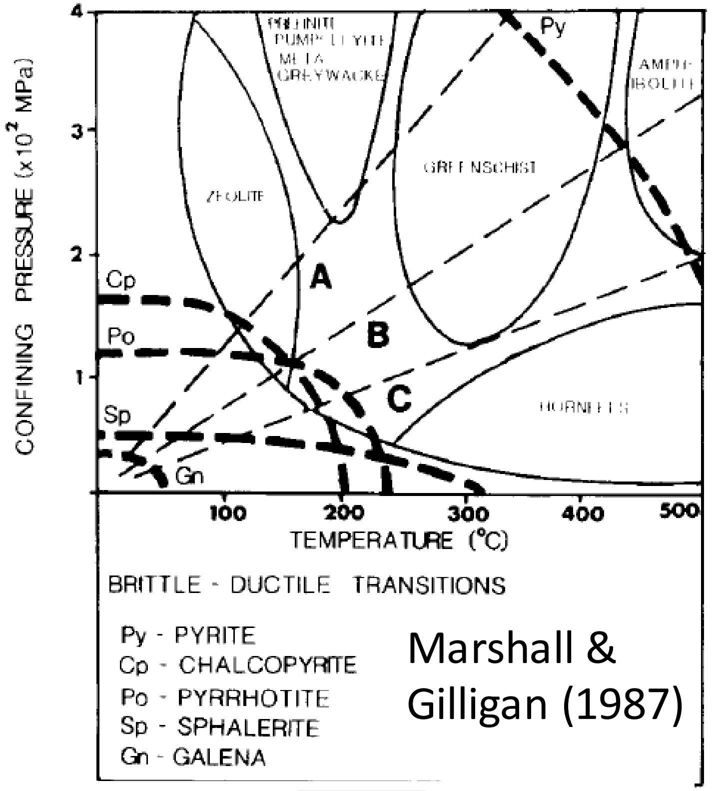

Marshall & Gilligan (1987)

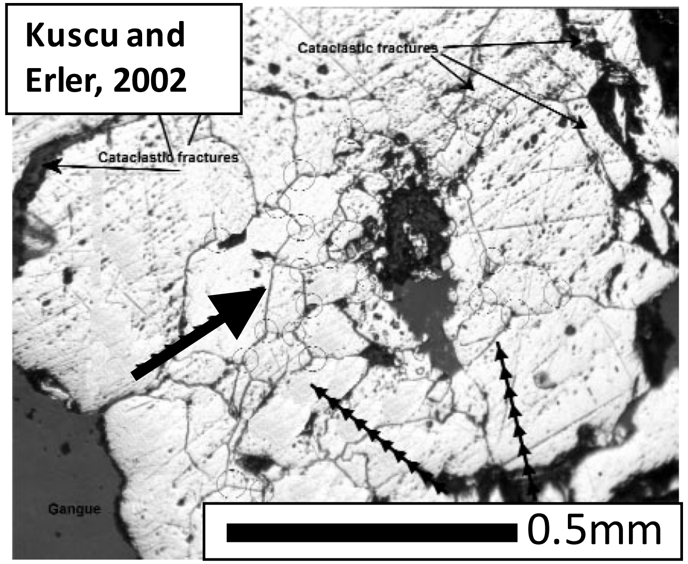

Kuscu and Erler, 2002

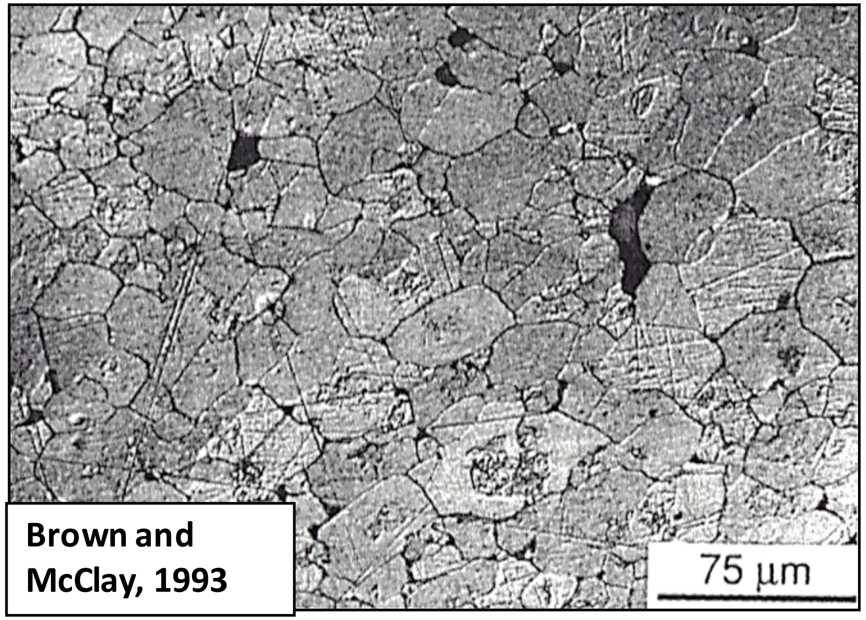

Brown and McClay, 1993

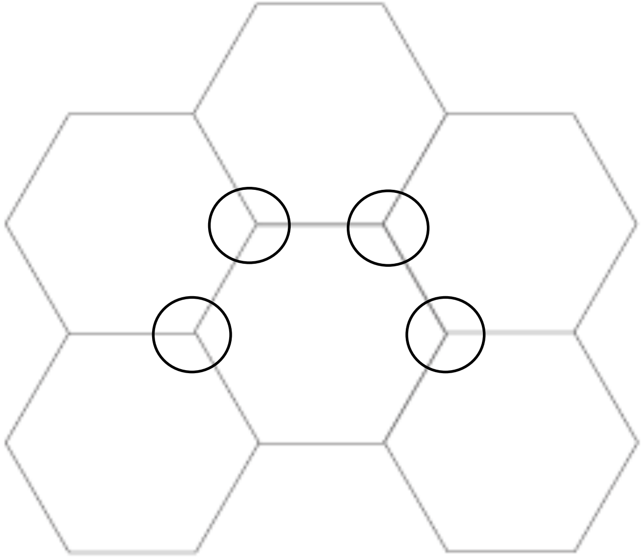

Foam textures in 550 °C amphibolite facies massive ore, Sulitjelma, Norway

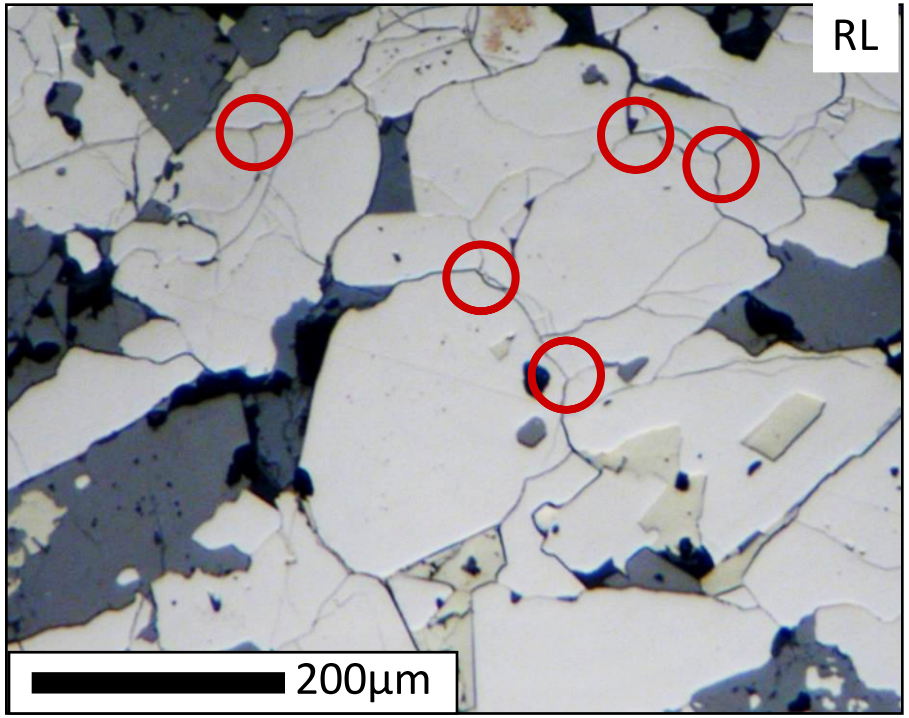

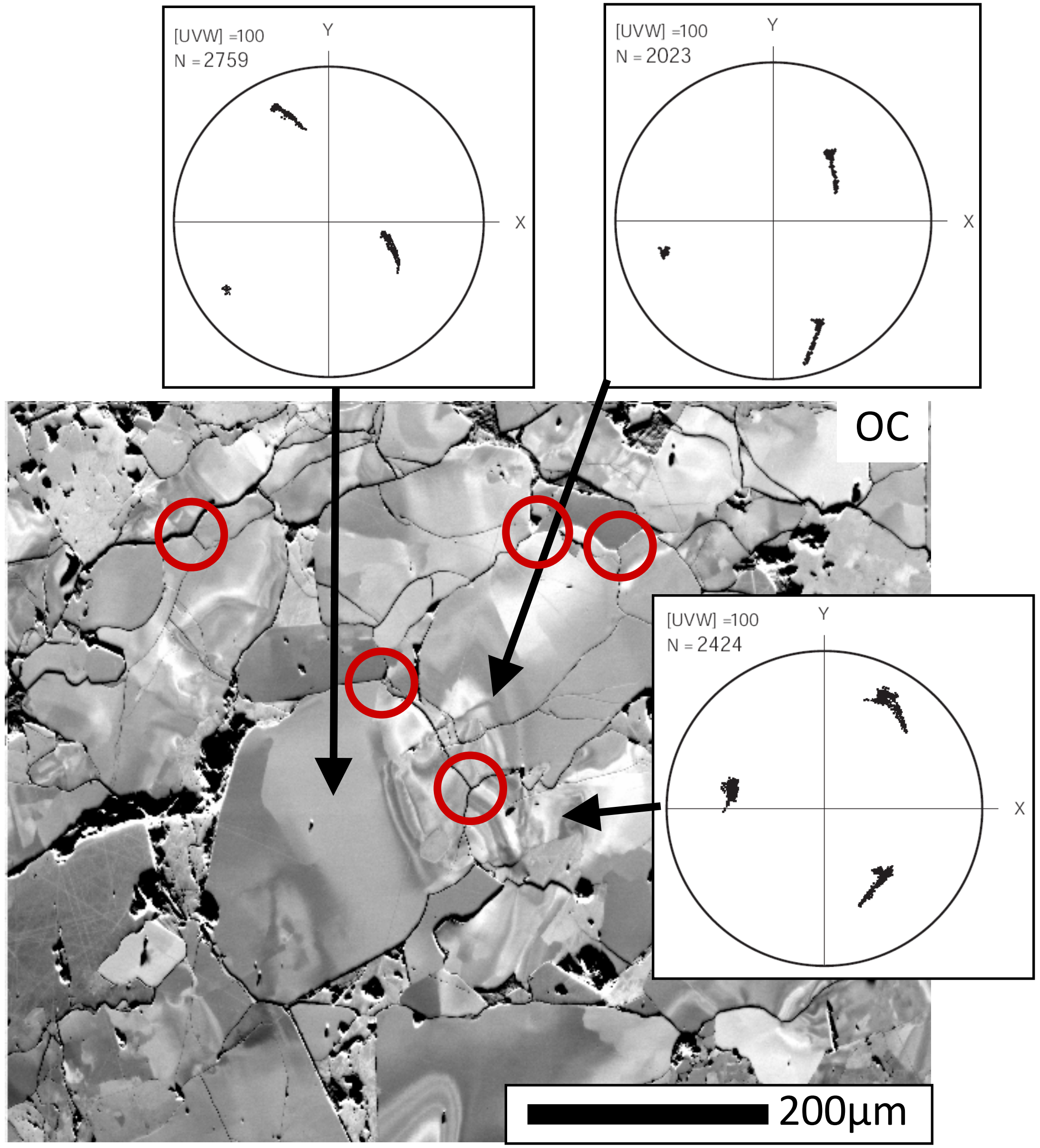

- Reflected light image suggest these are foam textures with some later brittle fractures.
- OC image indicates obvious plastic deformation within grains
- Textural equilibration at grain boundaries only?

Replacement textures – Pyr-Mt

- Pyrite commonly replaced by magnetite at low T in hydrous oxidising environments – especially during diagenesis and also in spoil heaps.
- Harlov et al (1997, JMG) also report very high temperature alteration of pyrite to magnetite

Remnant Pyrite Magnetite

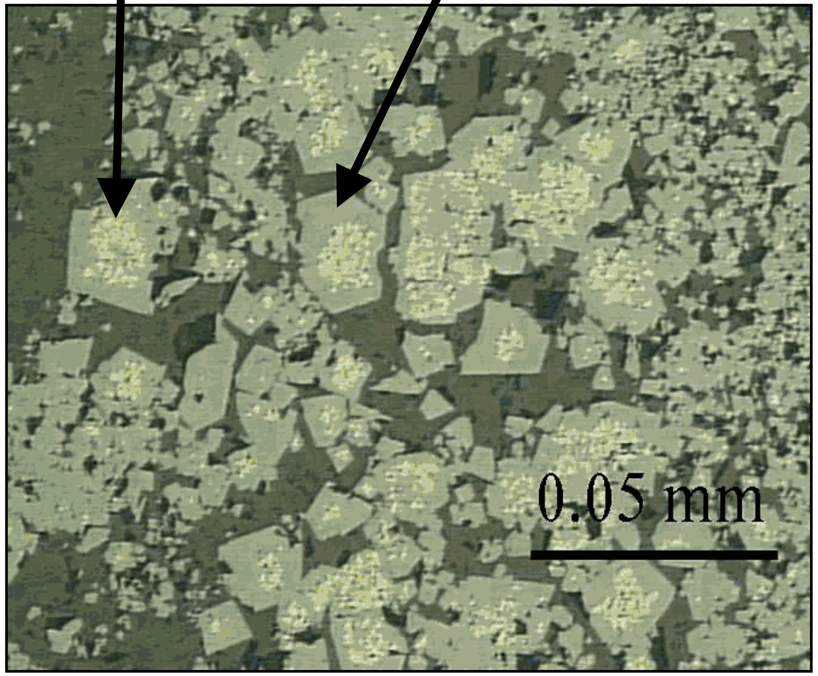

Remnant Pyrite Magnetite

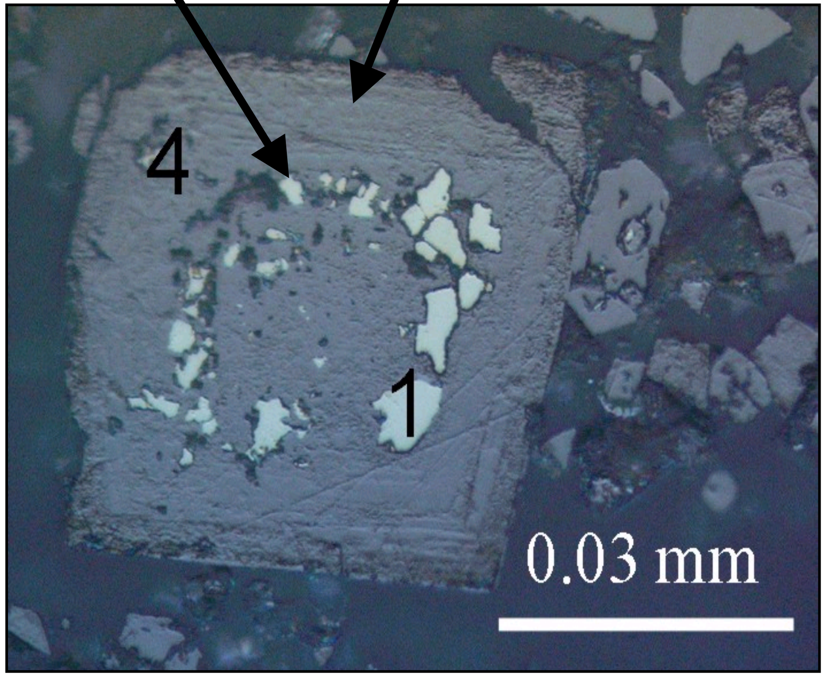

From: Sulphide-magnetitic ores from Sibay VHMS deposit (South Urals, Russia) - Zakis et al. web page.

Image of amphibolite facies magnetite with pyrite inclusions from Sulitjelma, Norway.

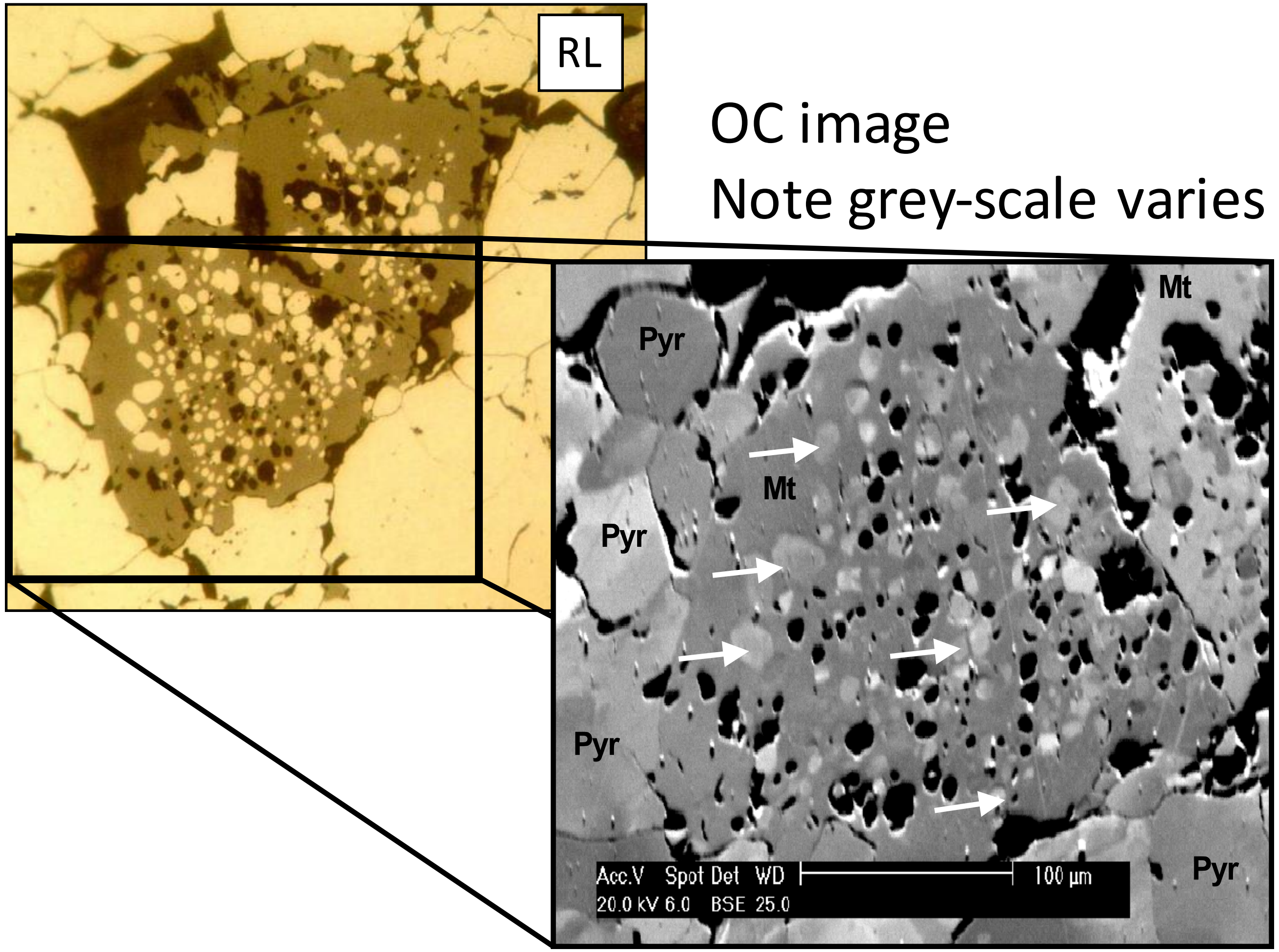

OC image
Note grey-scale varies

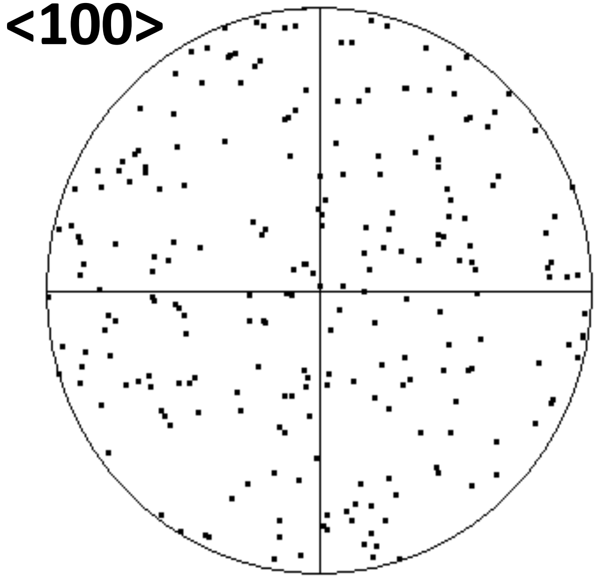

The pyrite <100> distribution is uniform/random - no simple pattern

Prior et al. 1999, American Mineralogist.

Reconstructed pyrite boundaries and crystal misorientation angles

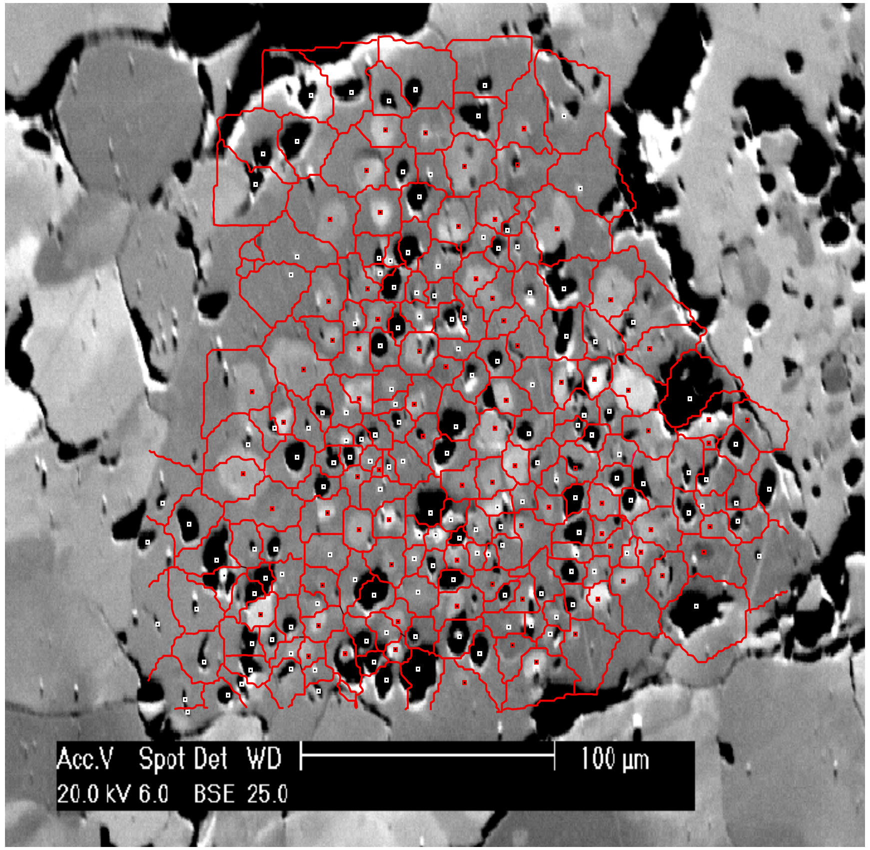

This is a random distribution

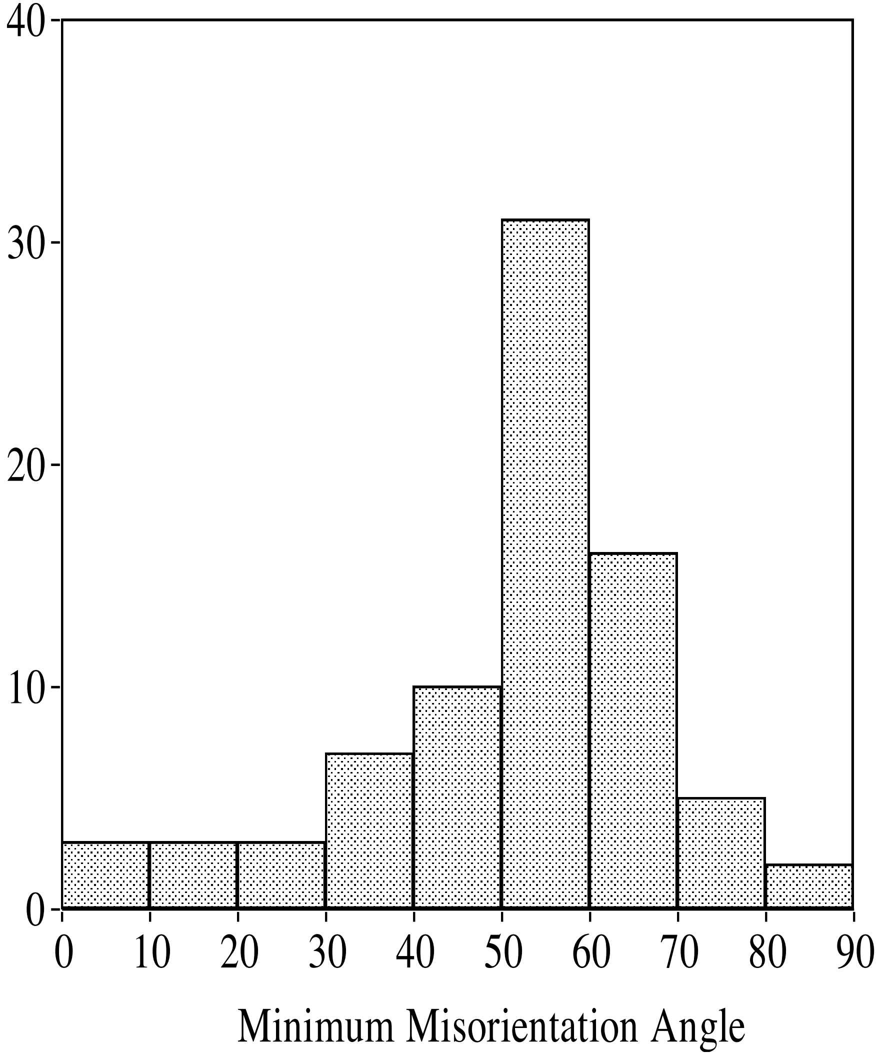

- Note that, despite cubic symmetry, the minimum misorientation angle for pyrite can be up to 90 degrees because <100> directions in pyrite are diad axes.

Prior et al. 1999, American Mineralogist.

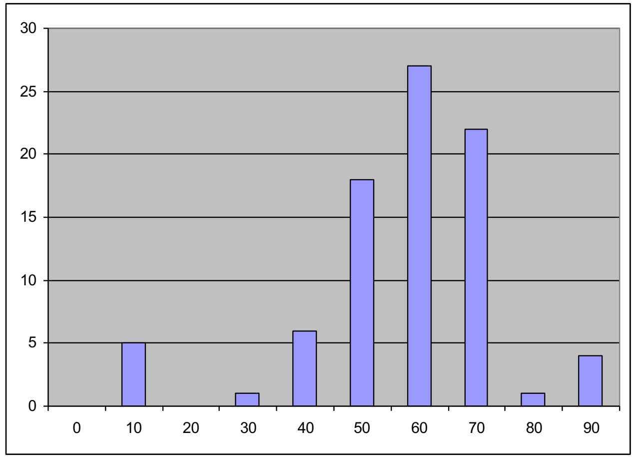

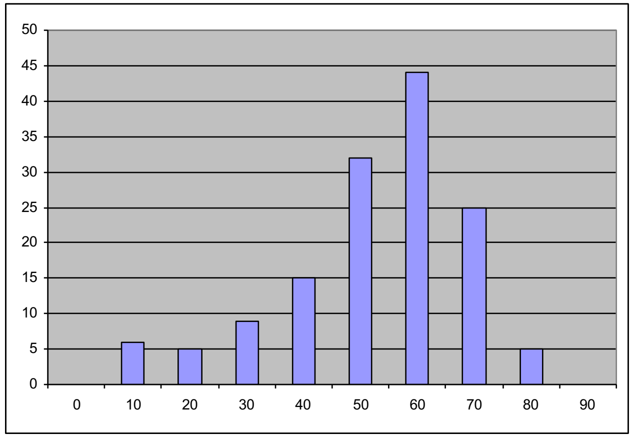

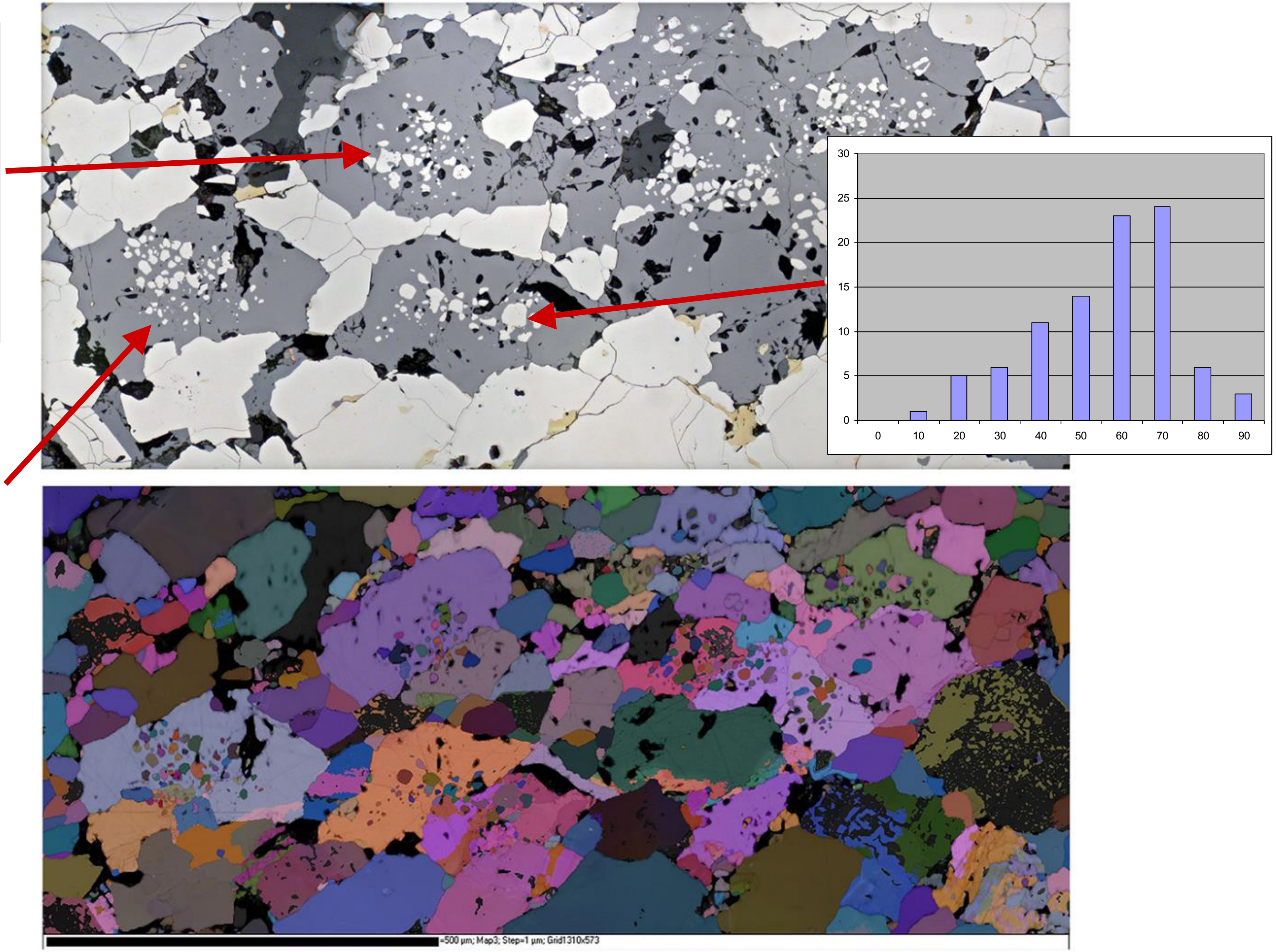

- Pyrite inclusions have random distributions

Possible mechanisms of formation

- Magnetite overgrows an early fine grained pyrite texture. Pyrite grain growth continues outside magnetite (c.f. quartz in garnet mica schists)?
  - Difficult to reconcile with pervasive plastic deformation of pyrite and lack of deformation of magnetite.
- Magnetite replaces pyrite porphyroblast and re-orients relict parts of original pyrite porphyroblast?
  - Difficult to conceive of a mechanism by which this may happen.
- Pyrite porphyroblasts locally 'shattered' into chaotic finer grained aggregate prior to magnetite replacement?
  - Oxidising fluid hydraulically fractures and shocks pyrite [amph facies].
  - 'Shocked' pyrite is more easily oxidised (Martello et al. 1994, GCA; Sasaki 1994, GCA).
  - Magnetite replaces along new grain boundaries.
  - 'Shock' consistent with evidence for high-T crack-seal structures in pyrite described by Boyle et al. (1998) Mineralium Deposita, 34, 71-81.

Evidence for high T fracturing/sealing of pyrite

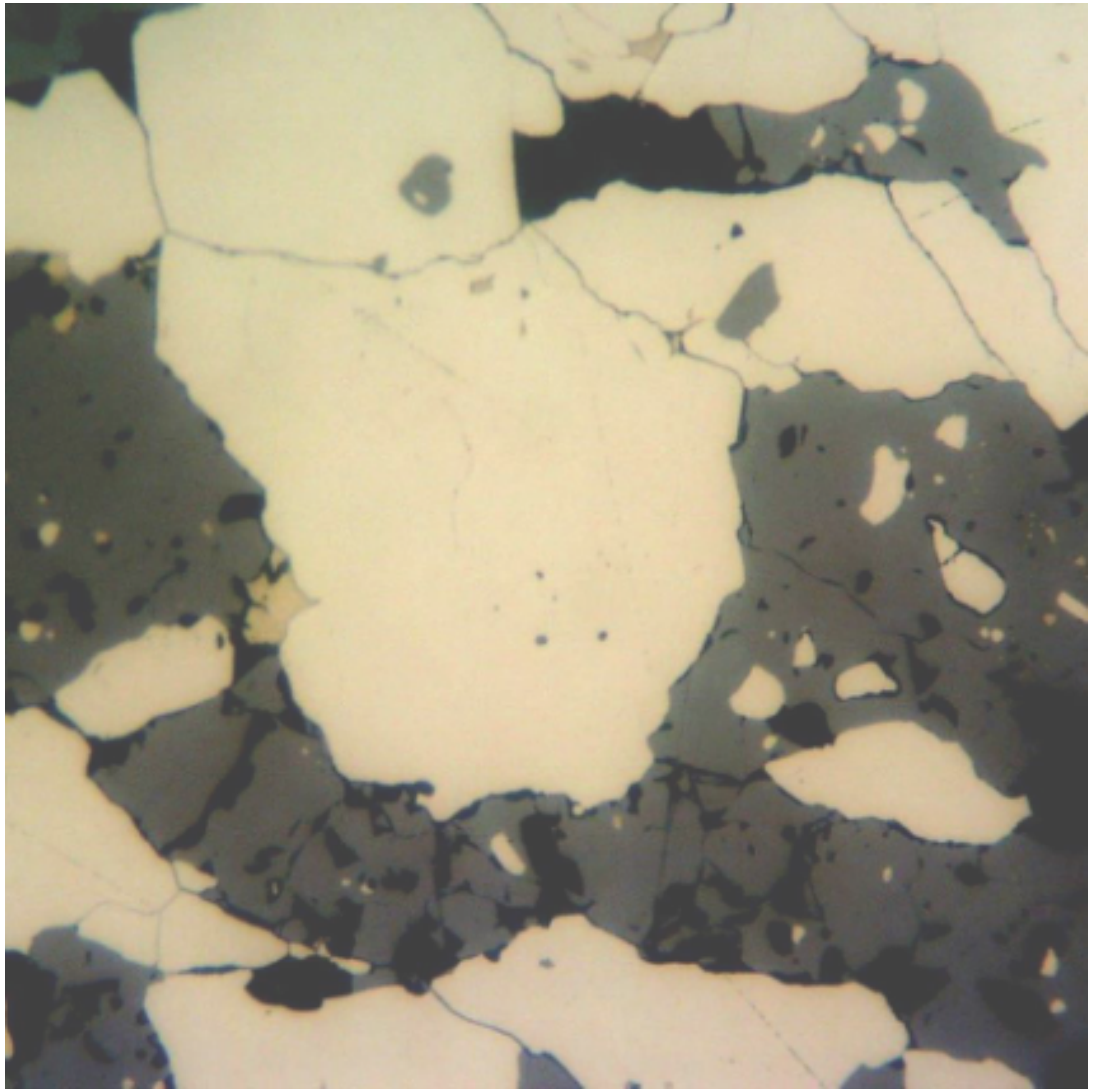

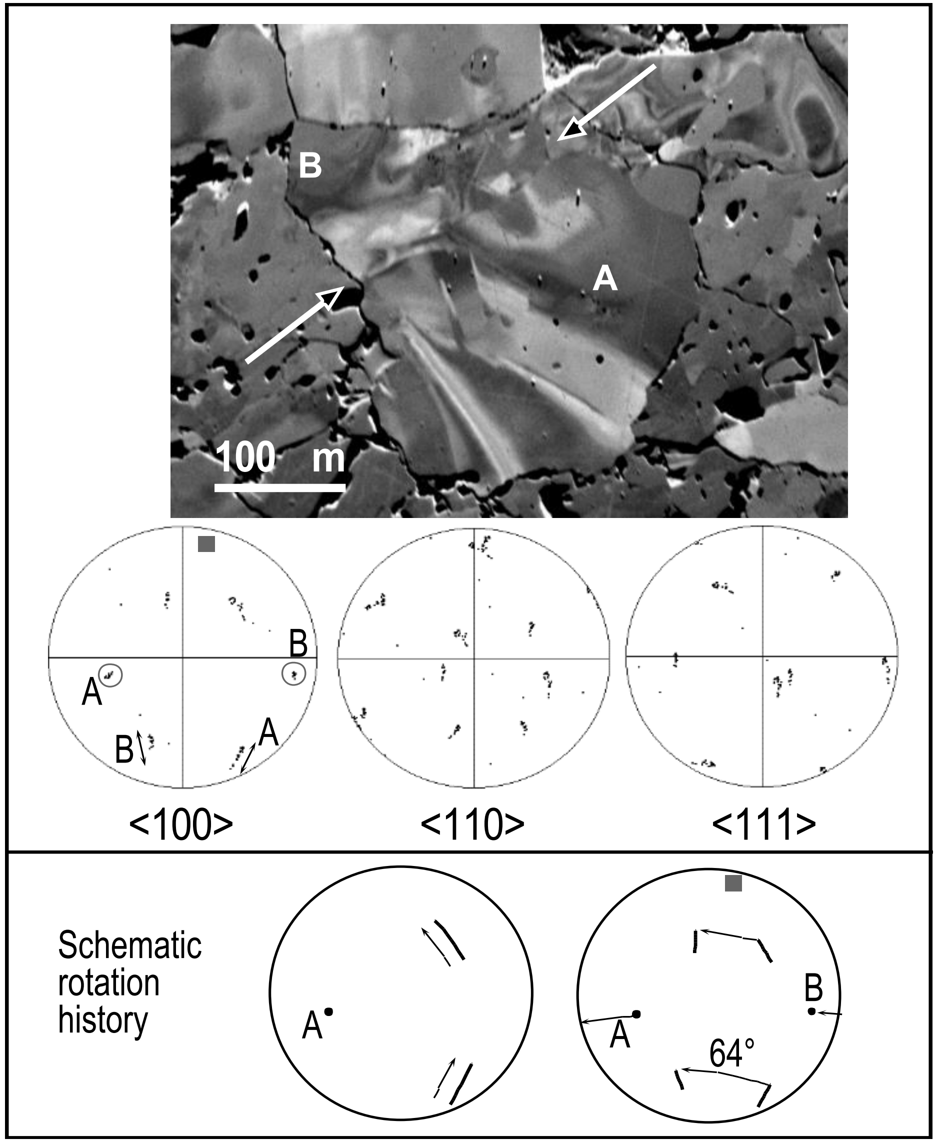

MSWM Jan 2004

Journal of the Geological Society, London, Vol. **166**, 2009, pp. 563–582. doi: 10.1144/0016-76492008-080.

On the growth of colloform textures: a case study of sphalerite from the Galmoy ore body, Ireland

CRAIG D. BARRIE[1,7]*, ADRIAN J. BOYCE[2], ALAN P. BOYLE[1], PATRICK J. WILLIAMS[3], KEVIN BLAKE[4], JAMIE J. WILKINSON[5], MIKE LOWTHER[6], PAUL MCDERMOTT[6] & DAVID J. PRIOR[1]

[1]*Department of Earth and Ocean Sciences, University of Liverpool, Liverpool L69 3GP, UK*

[2]*Scottish Universities Environmental Research Centre, Rankine Avenue, East Kilbride, Glasgow G75 0QF, UK*

[3]*EGRU, School of Earth and Environmental Science, James Cook University, Queensland 4811, Australia*

[4]*EGRU, Advanced Analytical Centre, James Cook University, Queensland 4811, Australia*

[5]*Department of Earth Science and Engineering, Imperial College London, Exhibition Road, London SW7 2AZ, UK*

[6]*Galmoy Mines Limited, Galmoy, Thurles, Co. Kilkenny, Ireland*

[7]*Present address: School of Geography and Geosciences, University of St Andrews, St Andrews KY16 9AL, UK.*

**Corresponding author (e-mail: cdb21@st-andrews.ac.uk)*

S-isotope and trace element variations in Galmoy sphalerite colloform…

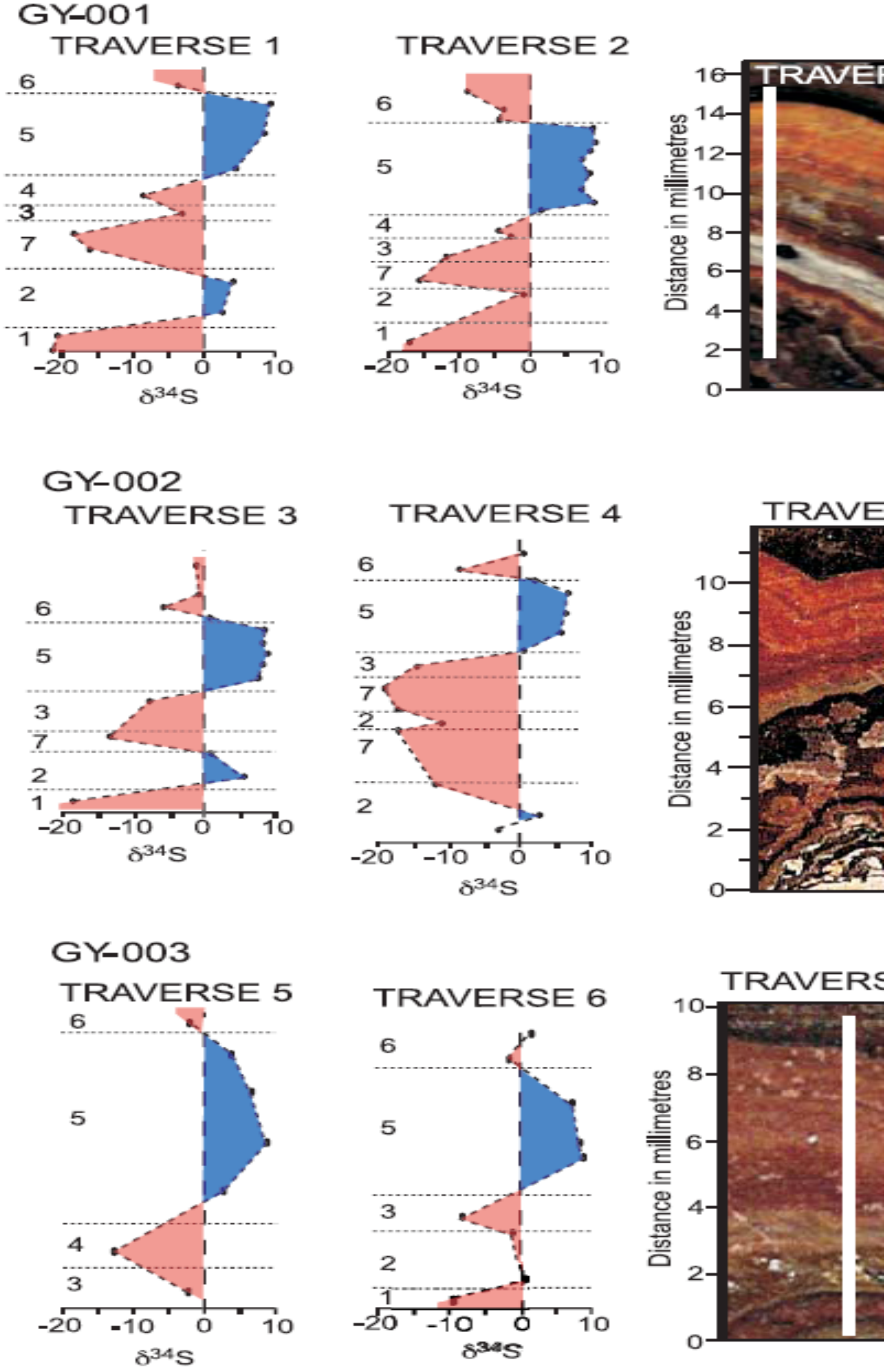

…indicate a dynamic fluid driven system

Fig. 9. Sulphur isotope transects of sphalerite, mapped perpendicular to the layering direction within each of the samples; the location of each traverse and layered stages are highlighted.

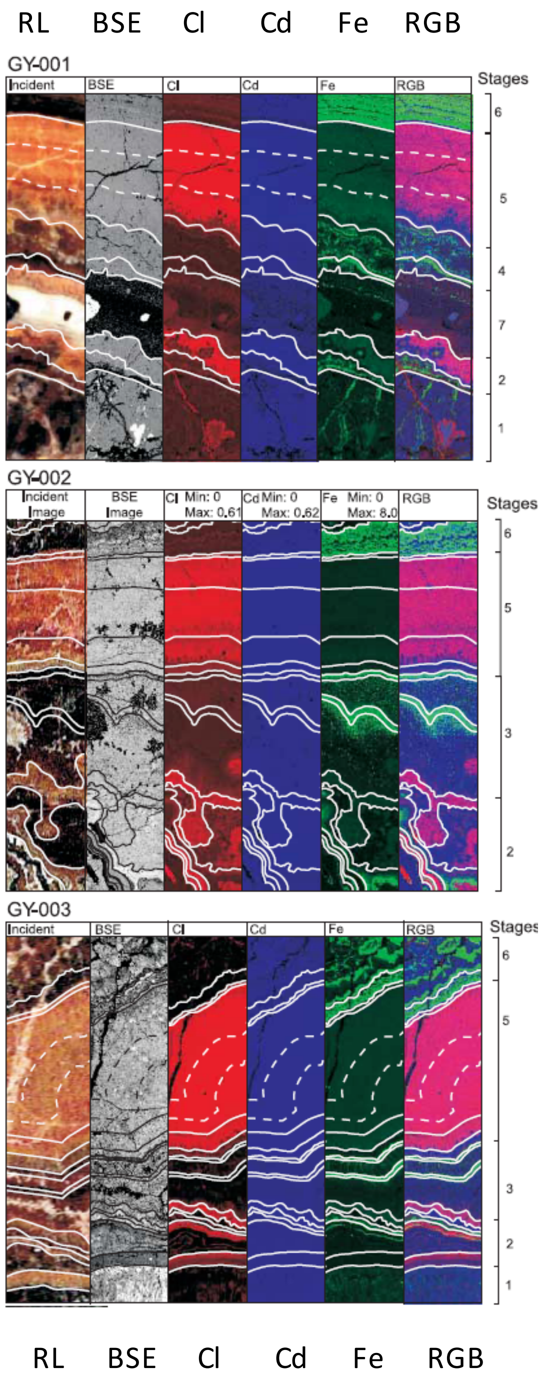

Fig. 11. Incident light, BSE images and trace element distribution maps for Cl (red), Cd (blue) and Fe (green) in all of the samples mapped; layering changes within each sample are highlighted, as are the stages that the layers belong to. Changes in colour brightness reflect differences in abundance. The red (Cl)–green (Fe)–blue (Cd) (RGB) composite map indicates where sequestration of more than one trace element has occurred within layers (e.g. purple indicates sequestration of both Cl and Cd, etc.). (a) GY-001; (b) GY-002; (c) GY-003. Minimum and maximum quantified results are given for each trace element for sample GY-002 in Table 1.

Sequence of sphalerite depositional layers record changing environmental conditions through time.

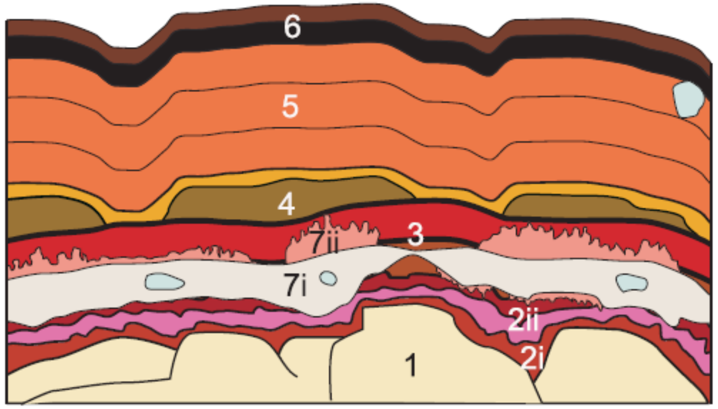

Fig. 5. Diagram illustrating the layering sequence within the colloform samples. Formation stages are highlighted in a proposed oldest to youngest sequence (stages 1–7).

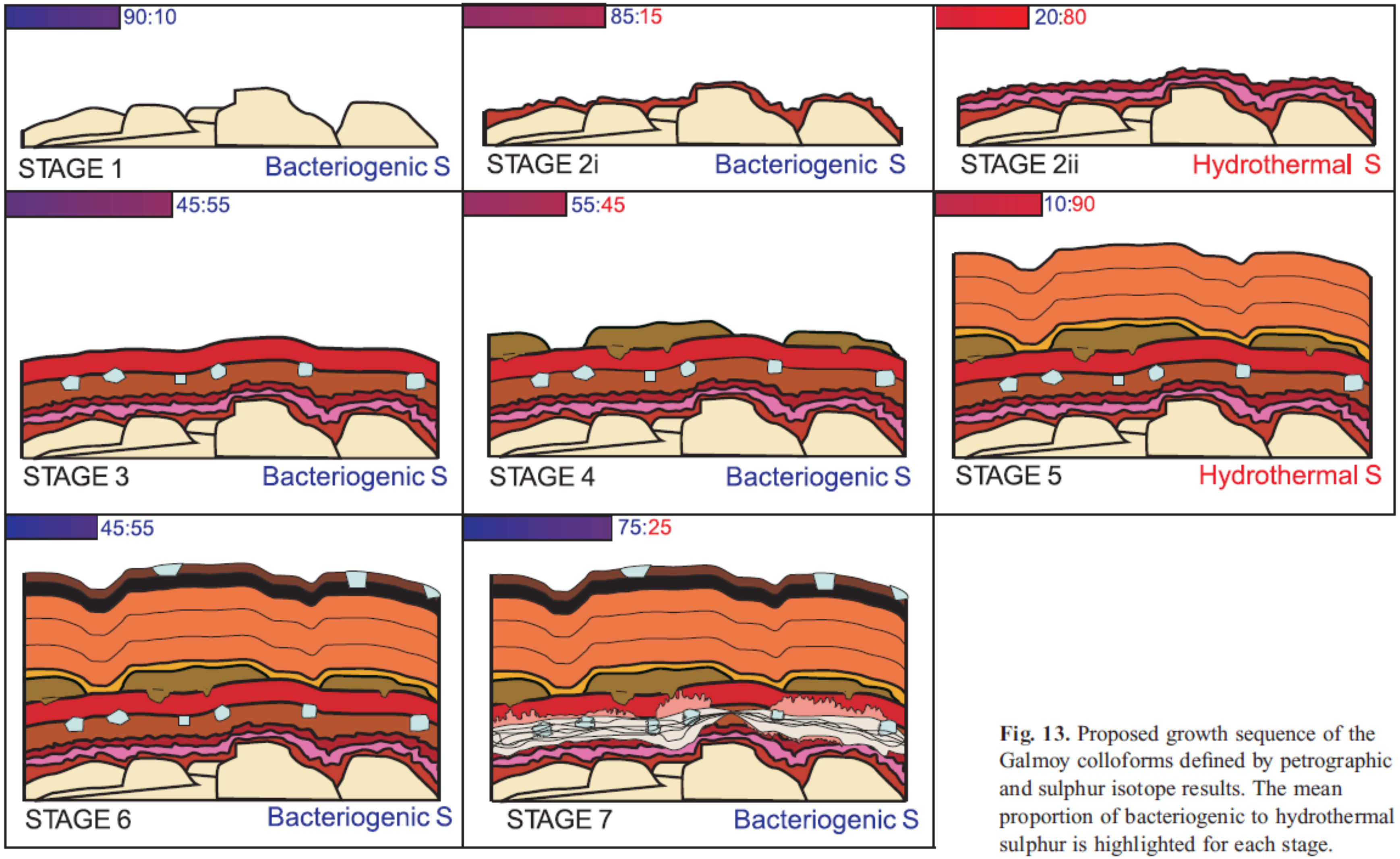

Fig. 13. Proposed growth sequence of the Galmoy colloforms defined by petrographic and sulphur isotope results. The mean proportion of bacteriogenic to hydrothermal sulphur is highlighted for each stage.

EBSD data

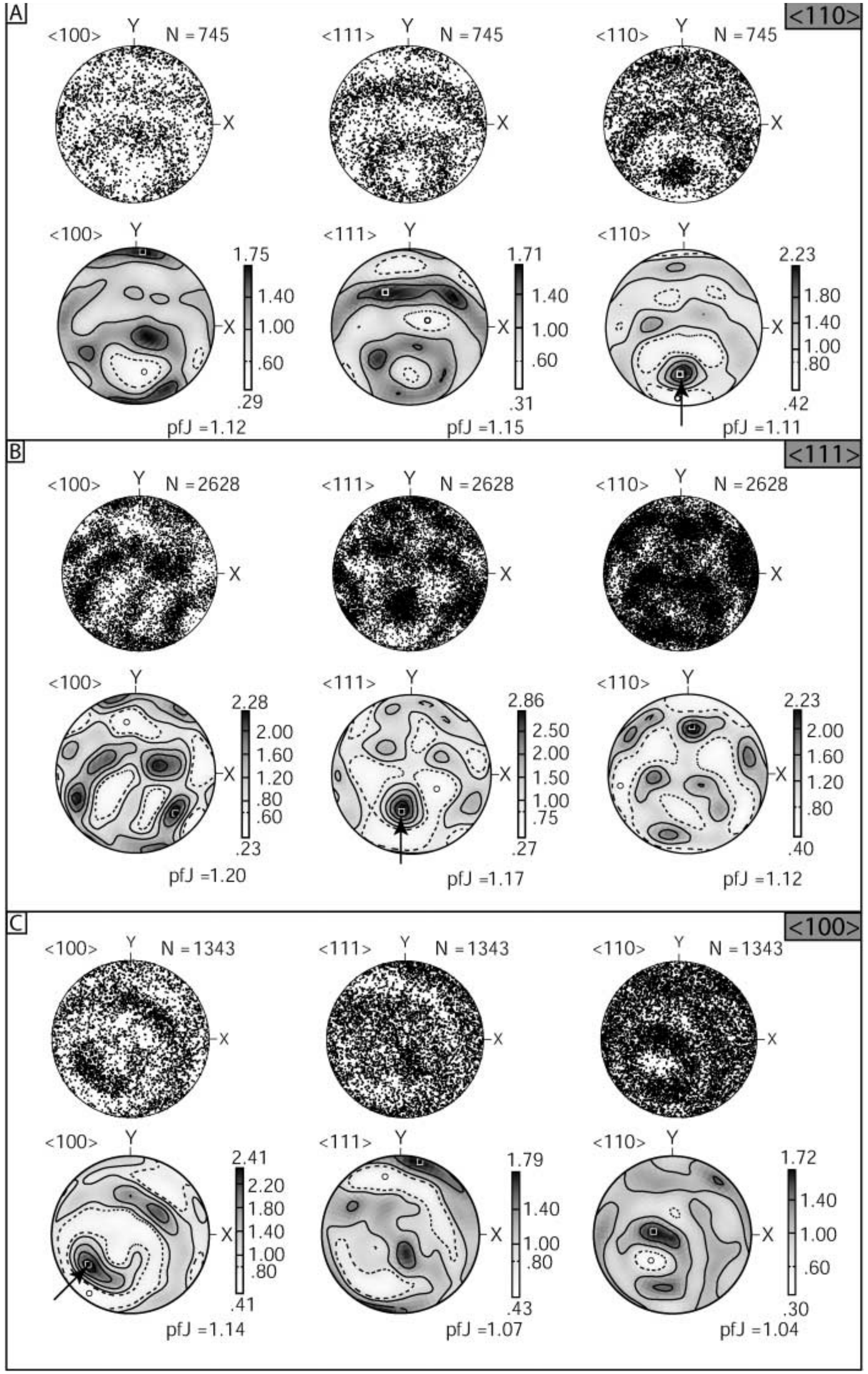

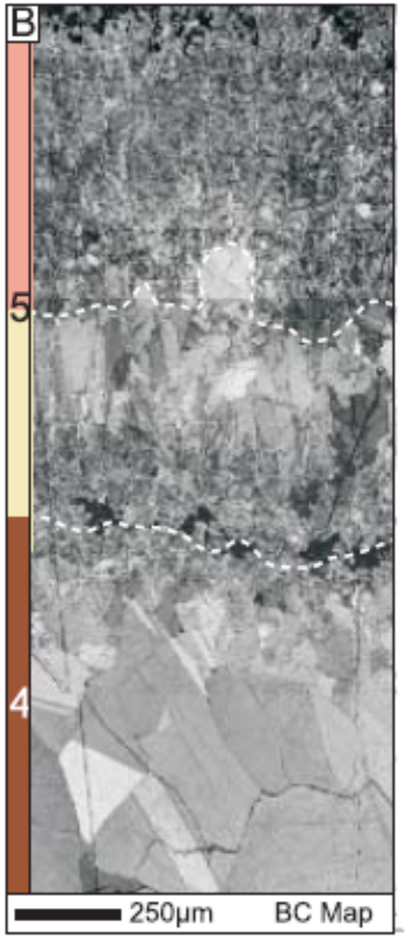

Self-organisation records evidence of changing supersaturation with time?

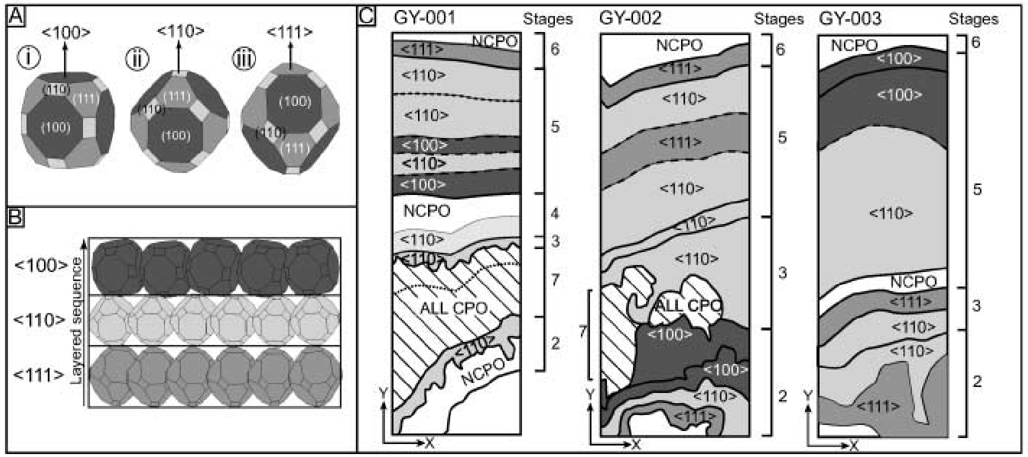

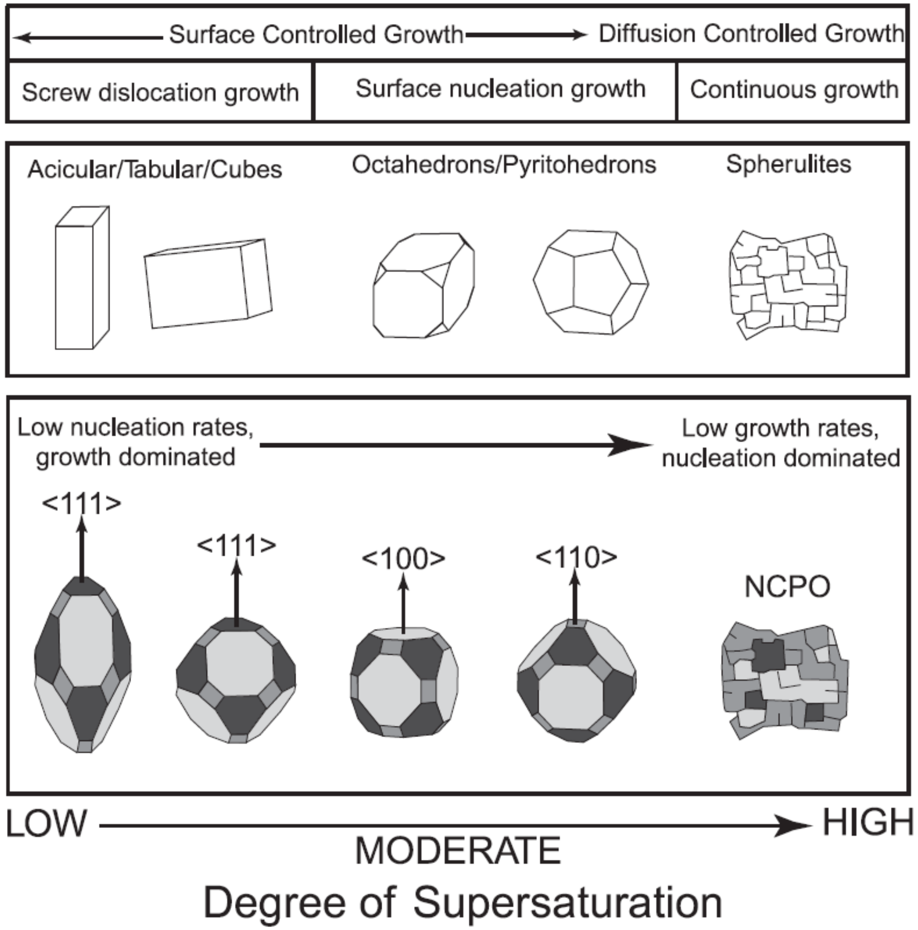

EBSD and quantifying deformation

ELSEVIER

Journal of Structural Geology 29 (2007) 1494–1511

JOURNAL OF STRUCTURAL GEOLOGY

www.elsevier.com/locate/jsg

An analysis of the microstructures developed in experimentally deformed polycrystalline pyrite and minor sulphide phases using electron backscatter diffraction

Craig D. Barrie*, Alan P. Boyle, David J. Prior

Department of Earth and Ocean Sciences, University of Liverpool, Liverpool, L69 3GP, UK

Received 9 January 2007; received in revised form 19 April 2007; accepted 14 May 2007
Available online 29 May 2007

Previous Work

- Samples are from the Blow ore body of the Mt Lyell Mining and Railway Company, Tasmania and were deformed in a gas apparatus rig by triaxial shortening.
- Results suggested that plastic deformation via dislocation glide mechanisms with significant amounts of recovery and recrystallisation (Cox et al., 1981)
- These results were utilised by McClay and Ellis (1983, 1984) to determine the strain rate contours for dislocation glide and creep in a pyrite deformation mechanism map
- Neutron Diffraction by Siemes et al. (1993) analysis suggested a weak <111> CPO at low temperatures changing to a <100> orientation at 700°C

Cox et al. (1981) experiments

Samples:

1 sample of the original starting material

4 samples deformed at varying temperature were analysed using EBSD to determine the deformation mechanism and microstructural development

1. B-1: Starting Material
2. Run 048: 550°C
3. Run 092: 600°C
4. Run 059: 650°C
5. Run 053: 700°C

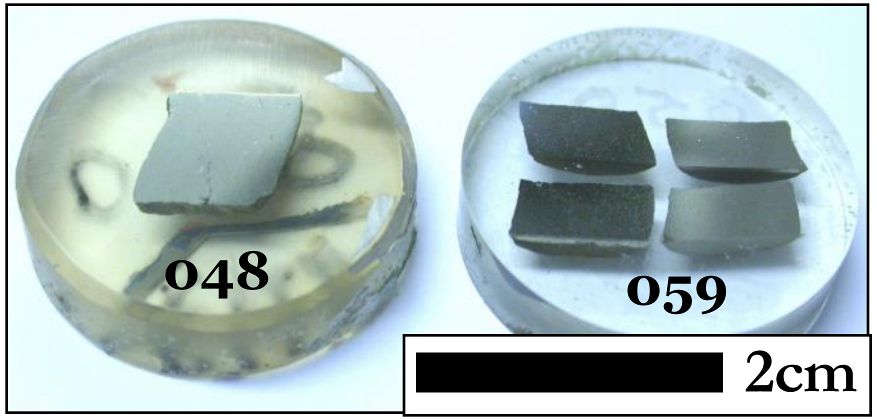

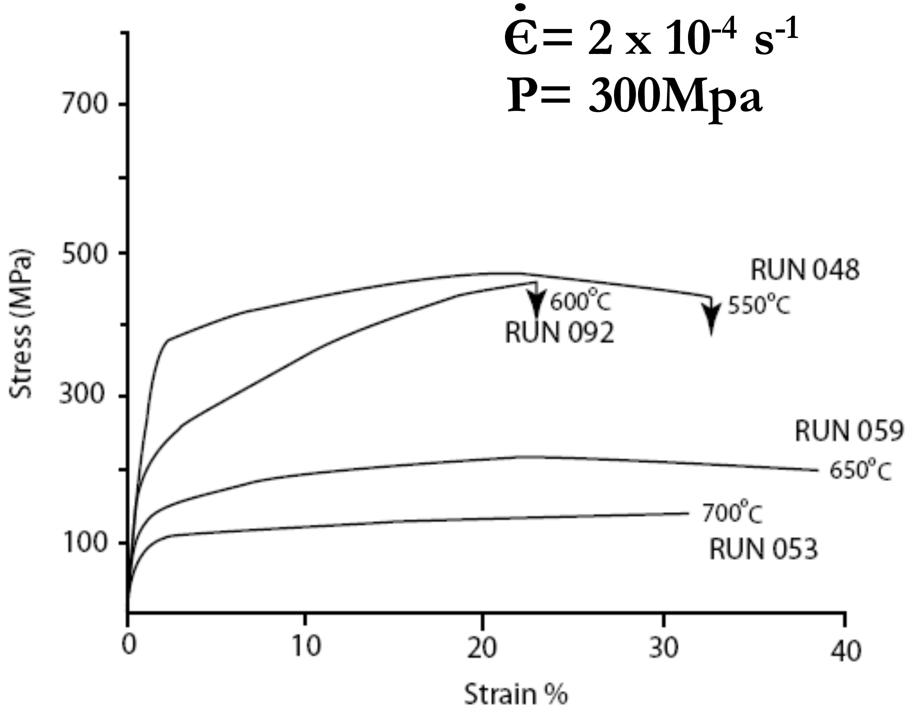

Within Grain Deformation

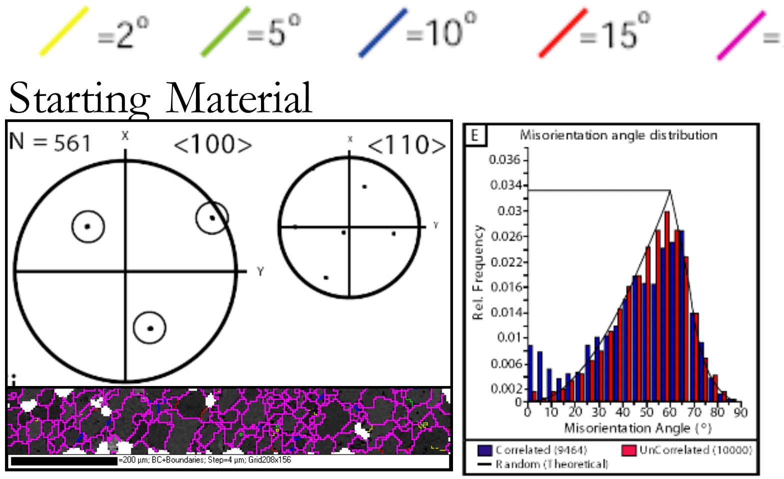

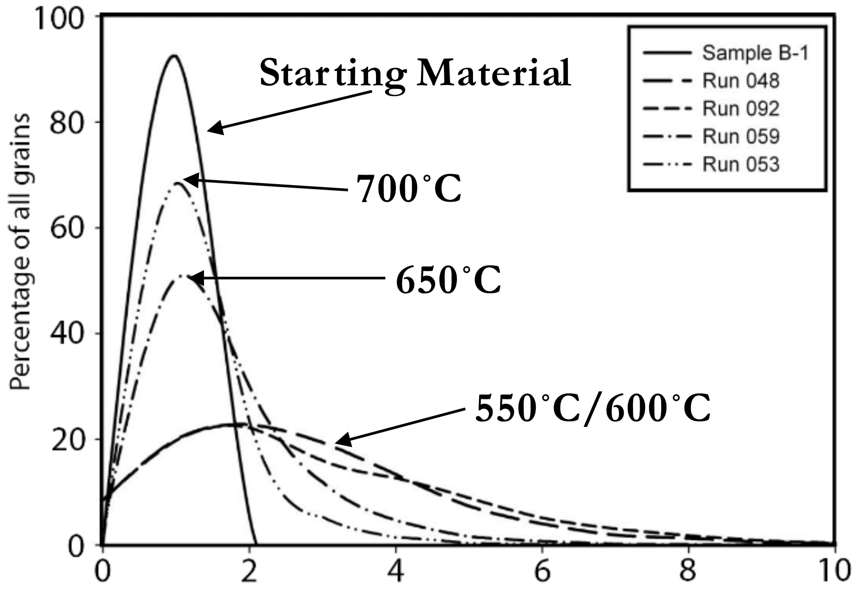

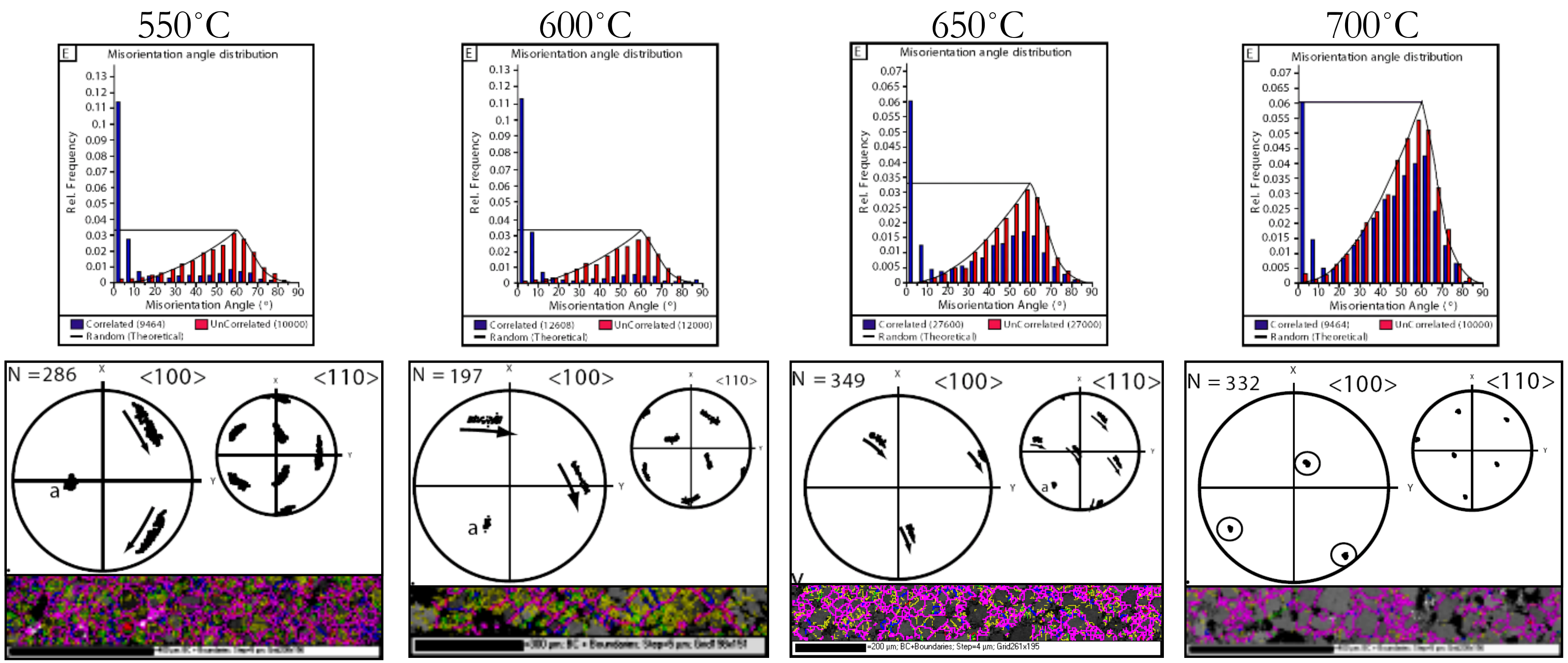

Starting material has ~1° intra-grain misorientation

550-600 °C deformation increases intra-grain misorientation and number of low angle grain boundaries.

650 °C deformation shows some recovery by recrystallisation.

700 °C deformation shows almost complete recovery to the starting material

Crystal Preferred Orientations?

Siemes et al. (1993) utilised Neutron diffraction to suggest that all of the samples up to 650˚C had an initial weak <111> CPO which altered to a <100> CPO at 700˚C (Siemes et al., 1993).

Maximum M.U.D. Minimum M.U.D.

However, all of the samples analysed in this study using EBSD to generate (1 point per grain) pole figures reveal a ‘random’ orientation of the crystals.

pfJ index of 1.0 = random distribution (Michibayashi and Mainprice, 2004)

There is no bulk CPO.

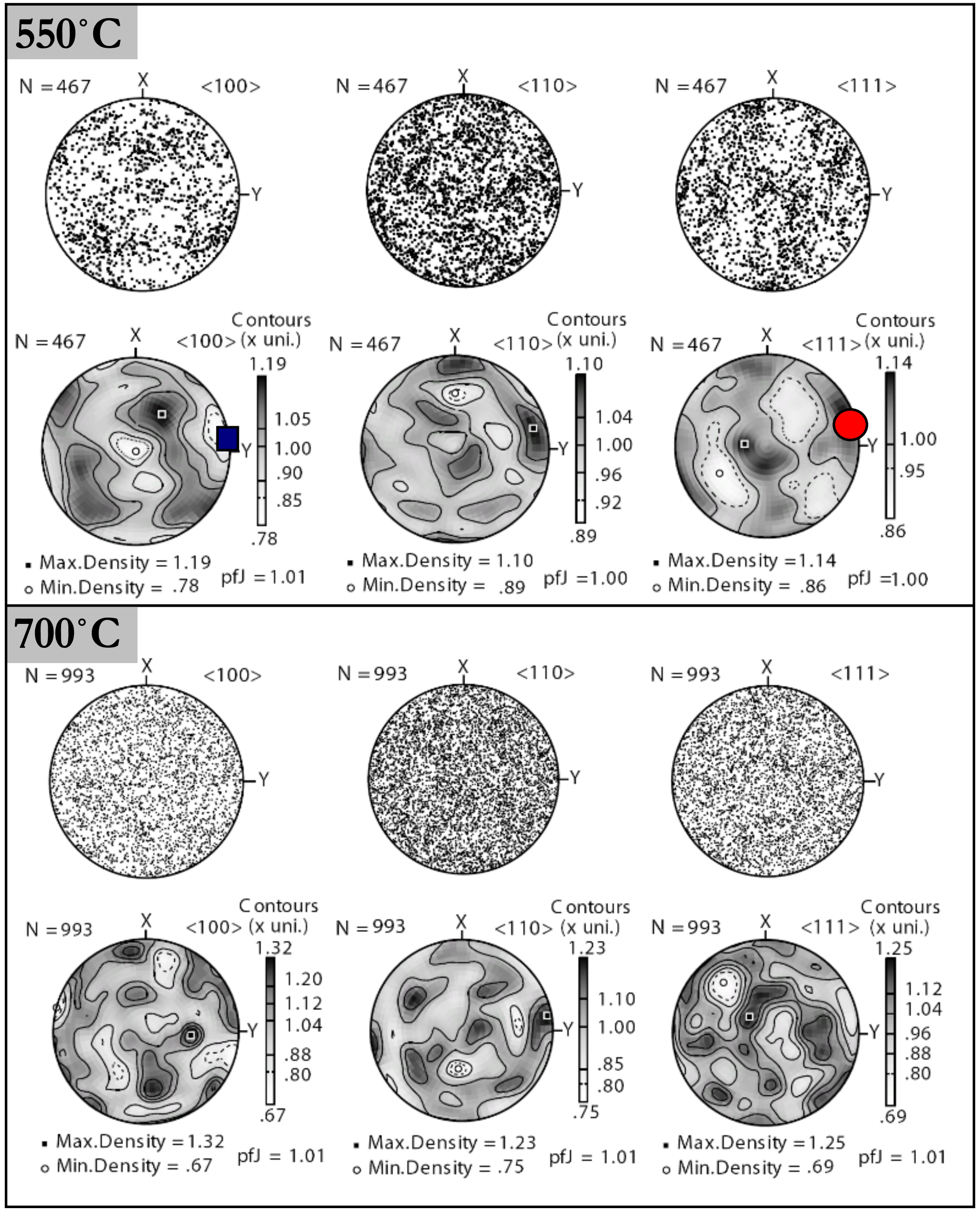

Recovery and recrystallisation

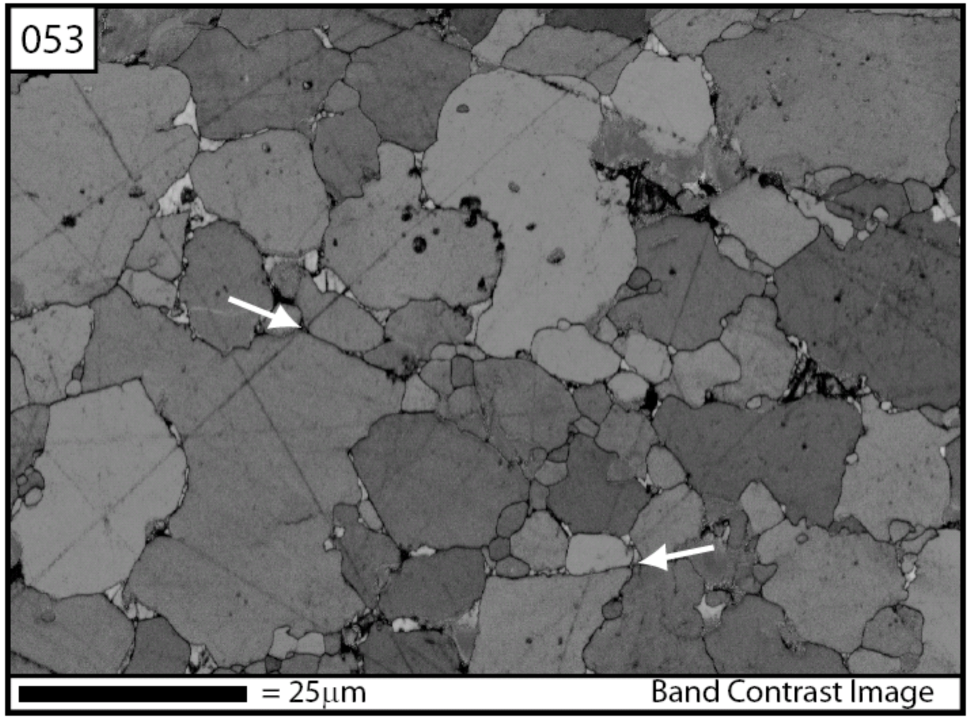

Pyrite deforms and recrystallizes in the same sort of regimes as the much more studied minerals like quartz.

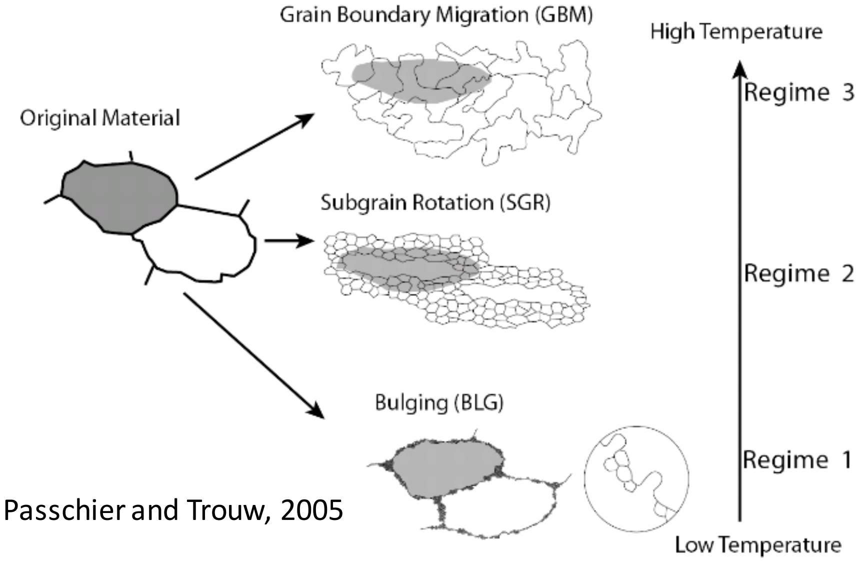

Passchier and Trouw, 2005

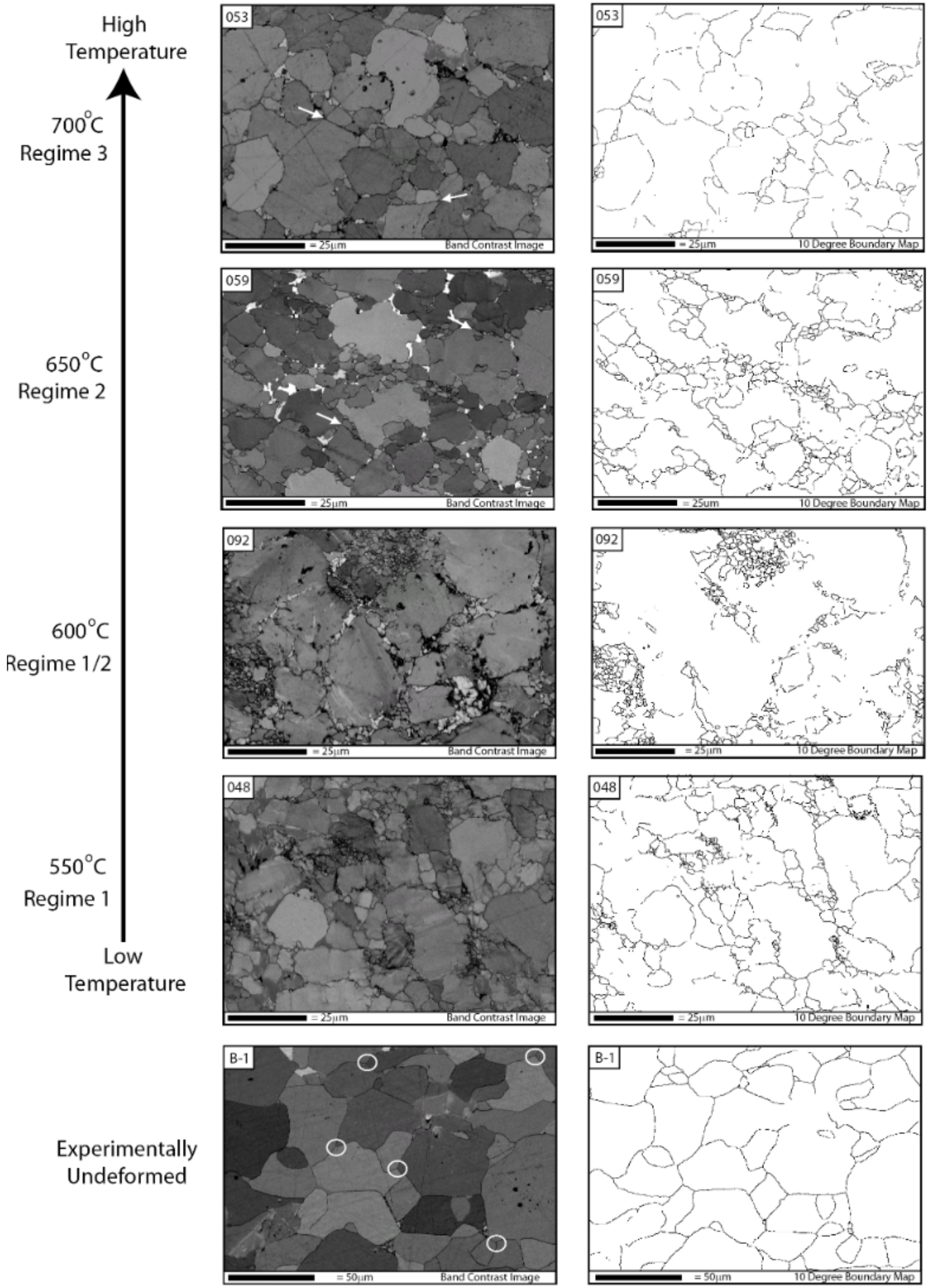

Implications

Between 550˚C and 700˚C at a strain rate of 2 x $10^{-4}s^{-1}$ and confining pressure of 300Mpa polycrystalline pyrite has **deformed via dislocation creep mechanisms**

Evidence for this deformation at high temperatures, however, has been partly removed by recrystallisation/recovery processes…

Recrystallisation processes change systematically with increasing temperature from **Blg** to **SGR** and finally **GBM**

These results did not fit with the existing deformation mechanism map for pyrite (McClay & Ellis, 1984)…

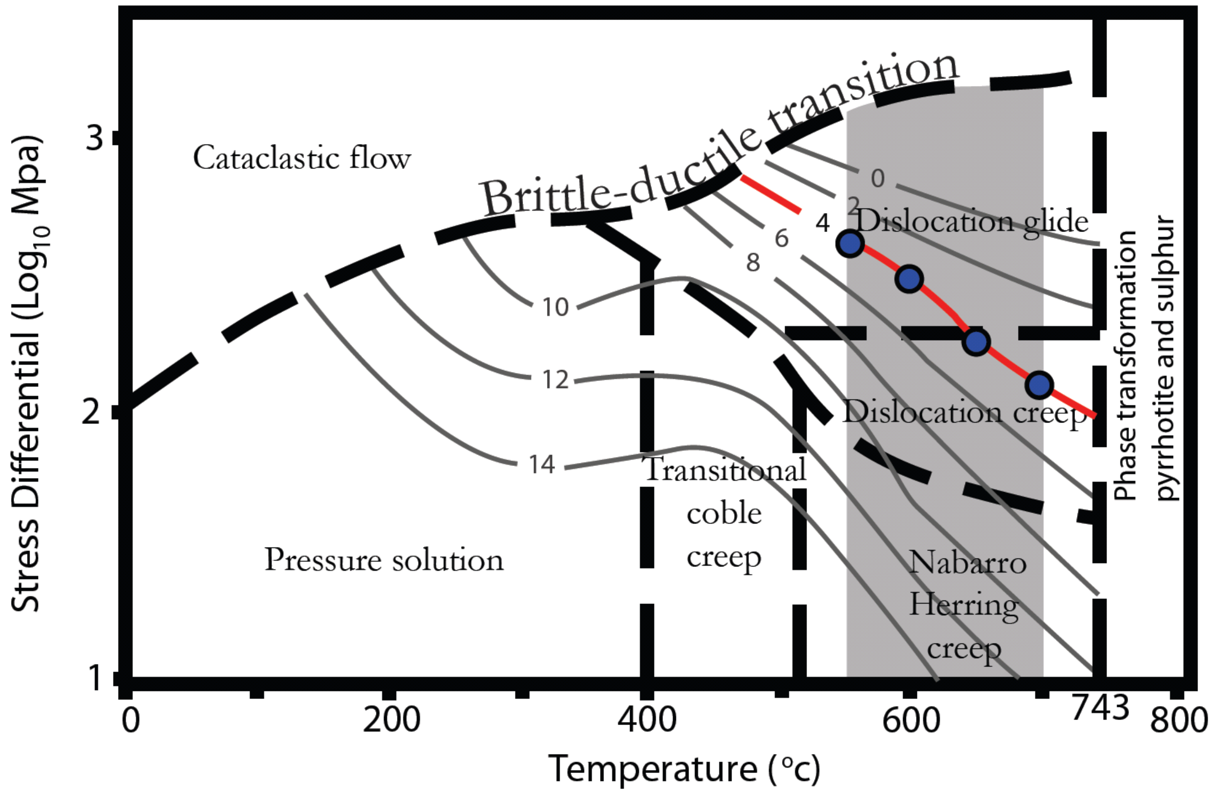

Deformation of pyrite in nature

Mineralogical Magazine, December 2009, Vol. 73(6), pp. 895–913

How low can you go? – Extending downwards the limits of plastic deformation in pyrite

C. D. Barrie[1,], A. P. Boyle[2] and M. Salter[2]

[1] School of Geography and Geosciences, University of St. Andrews, St. Andrews KY16 9AL, UK
[2] Department of Earth and Ocean Sciences, University of Liverpool, Liverpool L69 3GP, UK

[*Received 21 August 2009; Accepted 8 November 2009*]

Greens Creek, Alaska

~325 °C

Greens Creek Deposit: ~325°C, ~2–4.8kbar

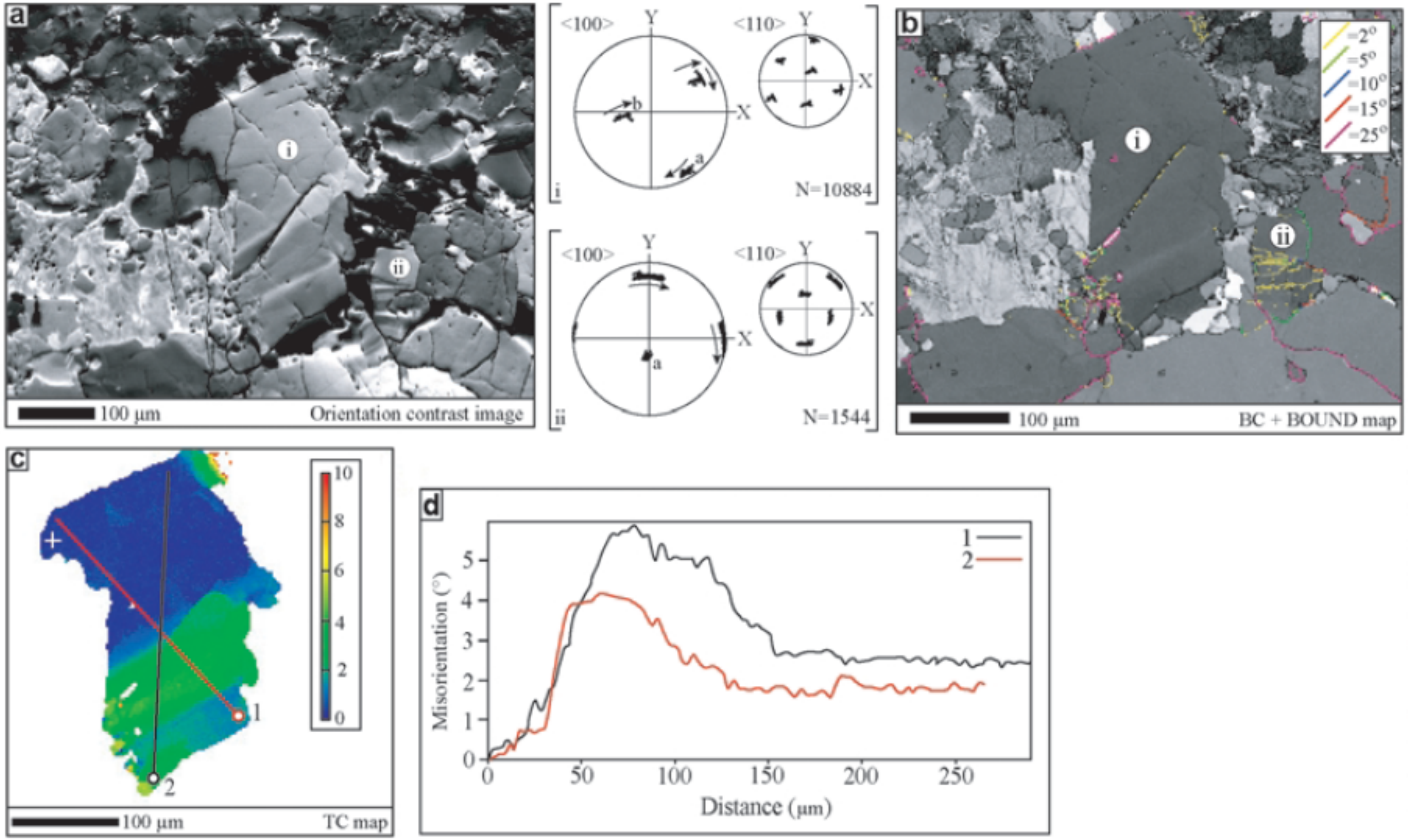

FIG. 6. Greens Creek Ore Deposit (~325ºC; ~2–4.8 kbar). (*a*) Orientation-contrast image with pole figures (i, ii) for selected pyrite grains; rotation direction is given by arrows and the rotation axis by a and/or b. (*b*) EBSD map showing the band-contrast image overlain by grain (~10–25º) and sub-grain (~2–10º) boundaries. (*c*) Texture-component (TC) EBSD map indicating lattice-misorientation changes in degrees, relative to a selected point (white cross), in the pyrite grain highlighted. (*d*) Cumulative-misorientation profiles for the EBSD transects (1 and 2) indicated in (*c*).

Løkken, Norway

~320 °C

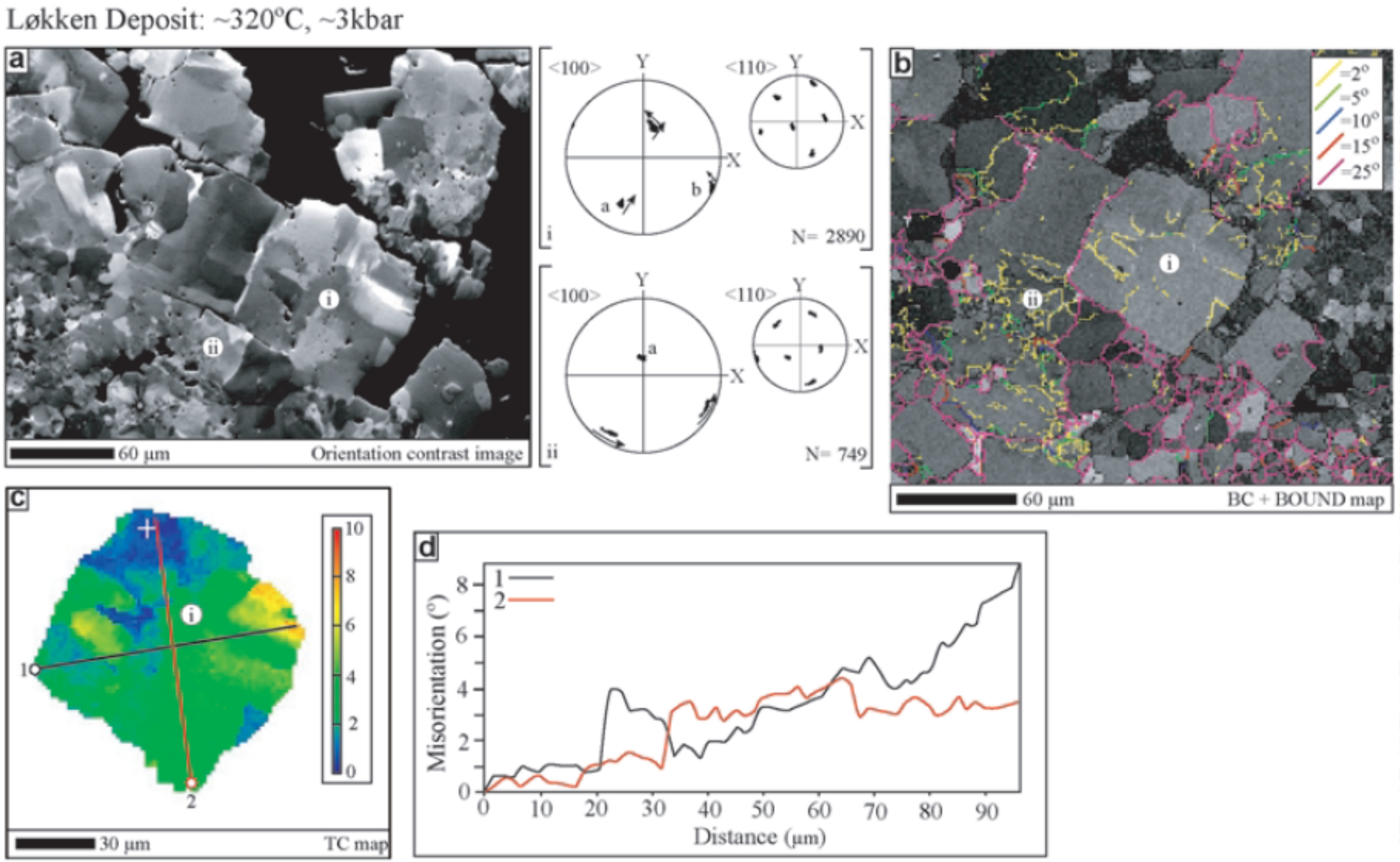

FIG. 5. Løkken Ore Deposit (~320ºC; ~3 kbar) (*a*) Orientation-contrast image with pole figures (i, ii) for selected pyrite grains; rotation direction is given by arrows and the rotation axis by a and/or b. (*b*) EBSD map showing the band-contrast image overlain by grain (~10–25º) and sub-grain (~2–10º) boundaries. (*c*) Texture-component (TC) EBSD map indicating lattice-misorientation changes in degrees, relative to a selected point (white cross), in the pyrite grain highlighted. (*d*) Cumulative-misorientation profiles for the EBSD transects (1 and 2) indicated in (*c*).

Parys Mountain, Angelsey

~200-260 °C

Dislocation creep in pyrite extends well below 500 °C

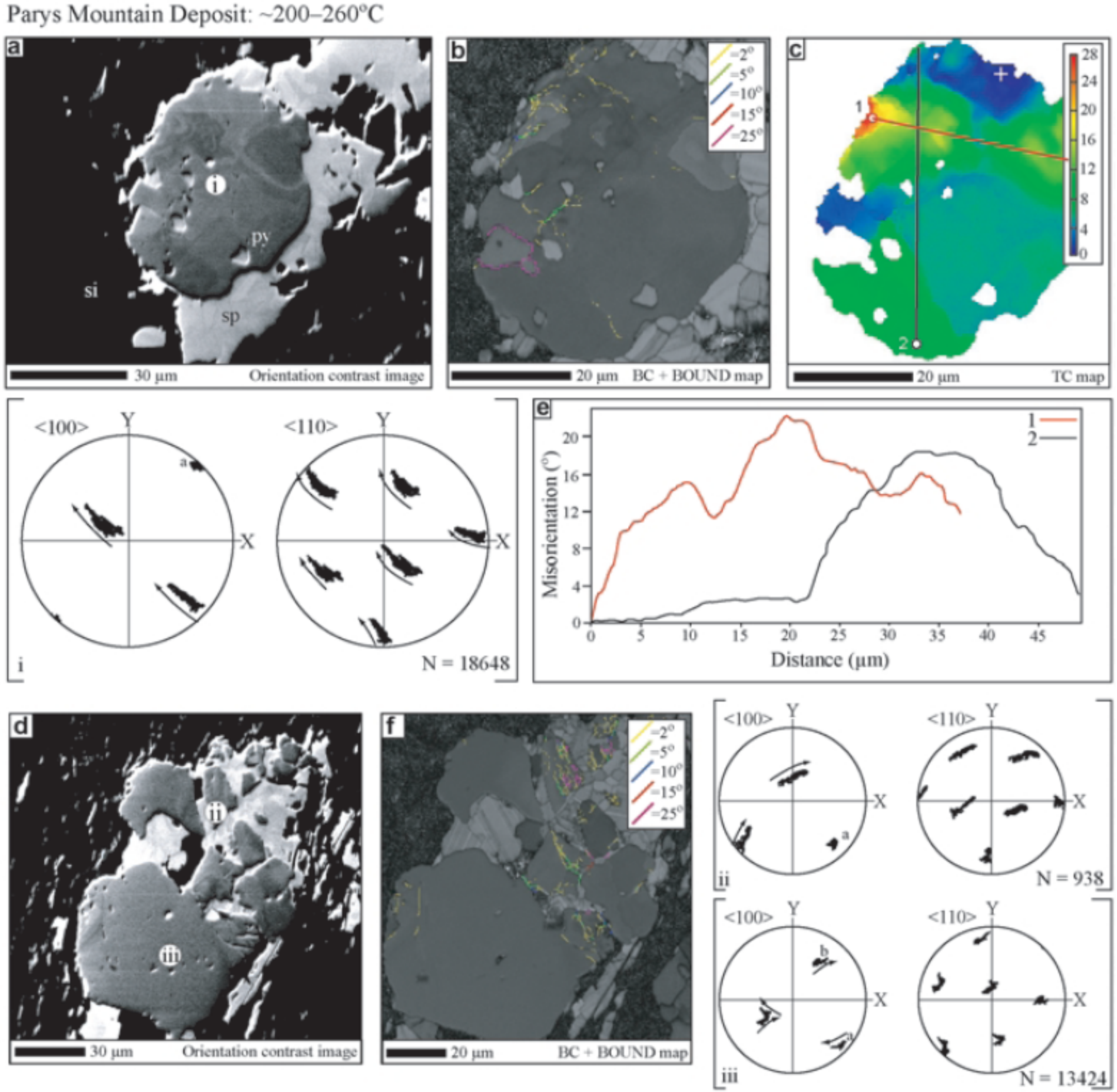

Tectonophysics 483 (2010) 269–286

Contents lists available at ScienceDirect

Tectonophysics

journal homepage: www.elsevier.com/locate/tecto

Pyrite deformation textures in the massive sulfide ore deposits of the Norwegian Caledonides

Craig D. Barrie [a,*], Alan P. Boyle [a], Nigel J. Cook [b], David J. Prior [a]

[a] *Department of Earth and Ocean Sciences, University of Liverpool, Liverpool, L69 3GP, United Kingdom*
[b] *School of Earth and Environmental Sciences, University of Adelaide, Adelaide, SA 5005, Australia*

Range of PT conditions

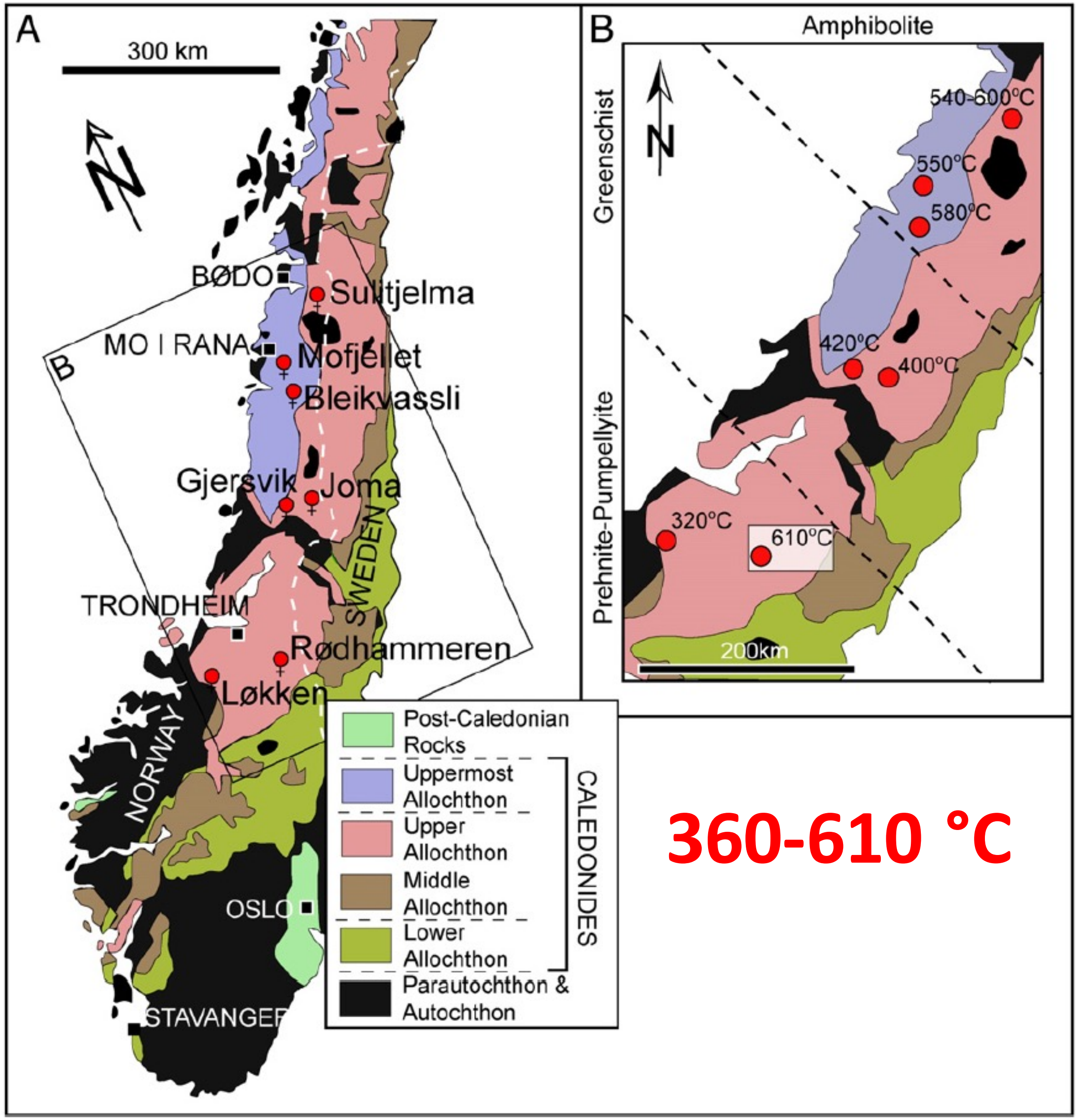

360-610 °C

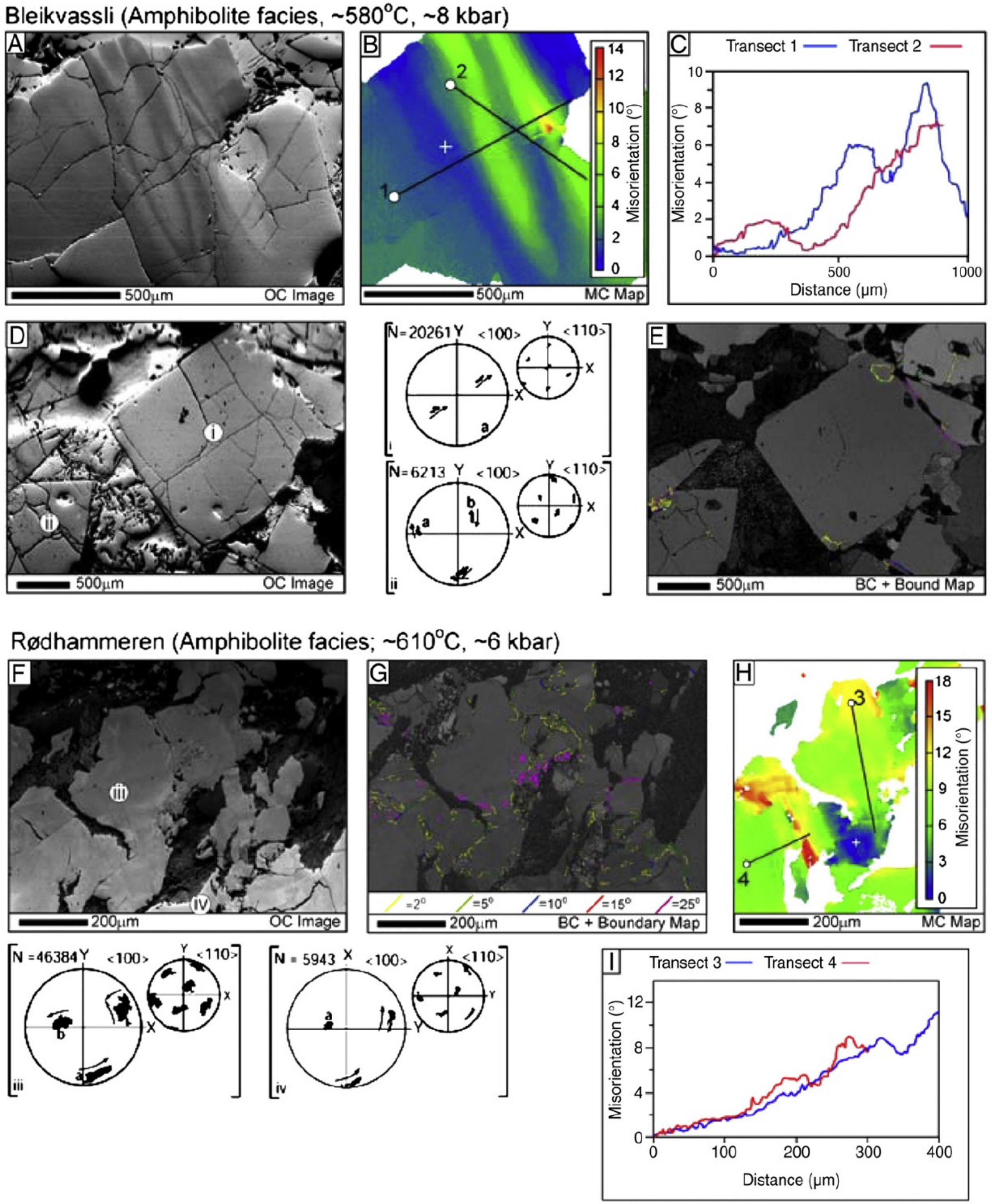

Ore Geology Reviews 39 (2011) 265–276

Contents lists available at ScienceDirect

Ore Geology Reviews

journal homepage: www.elsevier.com/locate/oregeorev

Reconstructing the pyrite deformation mechanism map

Craig D. Barrie [a,*], Mark A. Pearce [b], Alan P. Boyle [c]

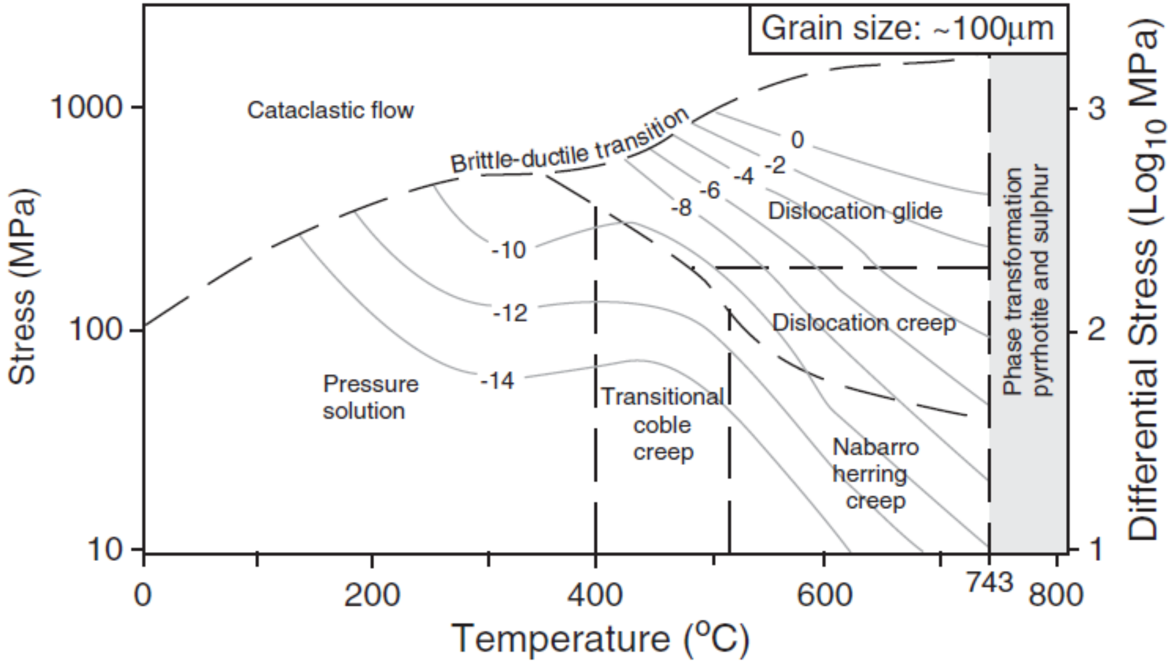

Fig. 1. The deformation mechanism map for polycrystalline pyrite with a grain size of ~100 µm published by McClay and Ellis (1983). Strain rate contours are in $10^{-n}s^{-1}$ and were defined using the results from Cox et al. (1981).

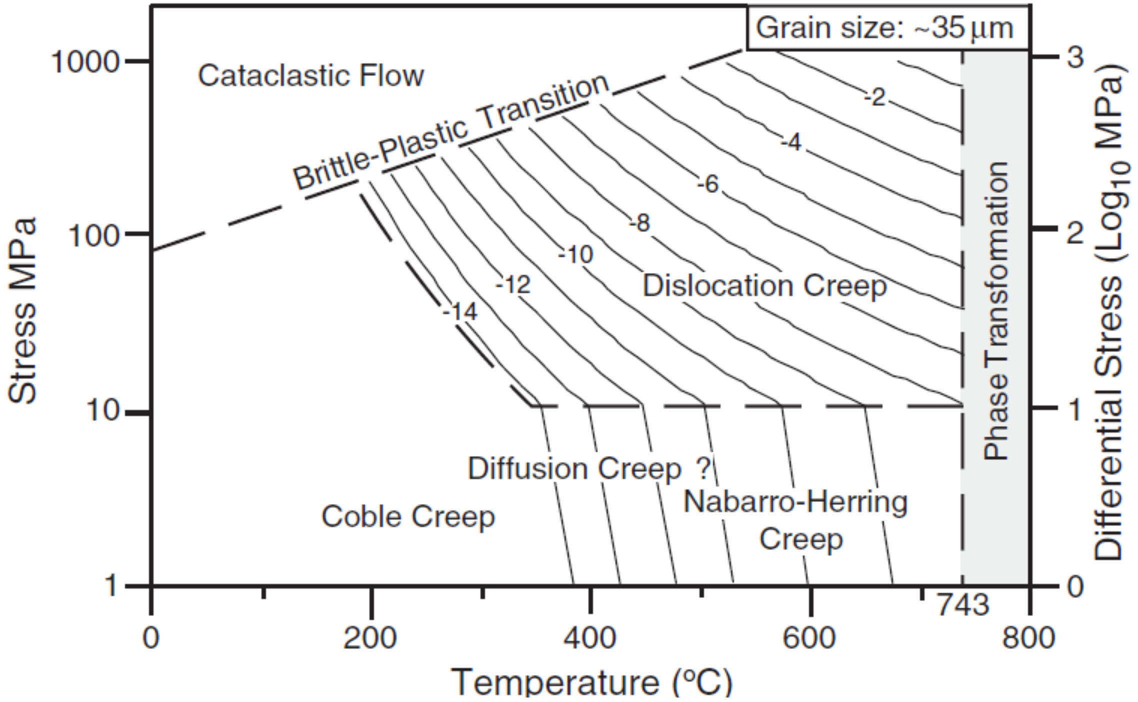

Fig. 10. The revised deformation mechanism map for polycrystalline pyrite with a mean grain size of ~35 µm, constructed using EBSD data from this and previous studies (Barrie et al., 2007, 2009, 2010a). The contours on the map are strain rate in units of $10^{-n}s^{-1}$ and were calculated using the original experimental stress–strain curves, some of which were presented in Cox et al. (1981).

How can this be used?

San Andreas Fault Observatory at Depth (SAFOD)

- Drilling experiment that cored through the San Andreas Fault at a depth of ~2.7km.
- Temperature in the observatory is ~120 °C
- Gouge and clay minerals are consistent with 120 °C
- Pyrite would be expected to have deformed by brittle mechanisms

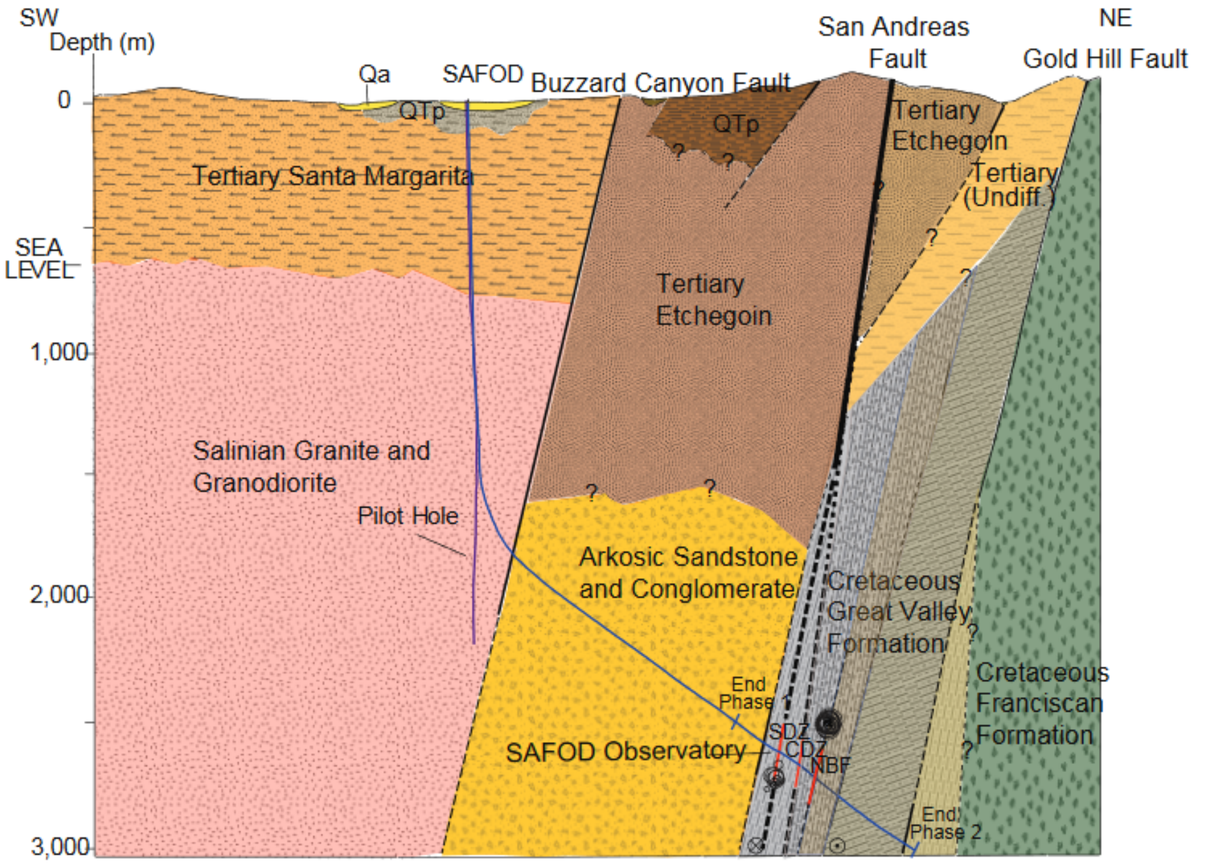

Figure 3. Simplified geologic cross-section parallel to the trajectory of the San Andreas Fault Observatory at Depth (SAFOD) borehole. The geologic units are constrained by surface mapping and the rock units encountered along both the main borehole and the pilot hole. The black circles represent repeating microearthquakes. The three notable fault traces associated with the San Andreas Fault damage zone (SDZ, CDZ, and NBF) are shown in red. The depth at which the SAFOD observatory is deployed is shown.

Zoback et al (2011)

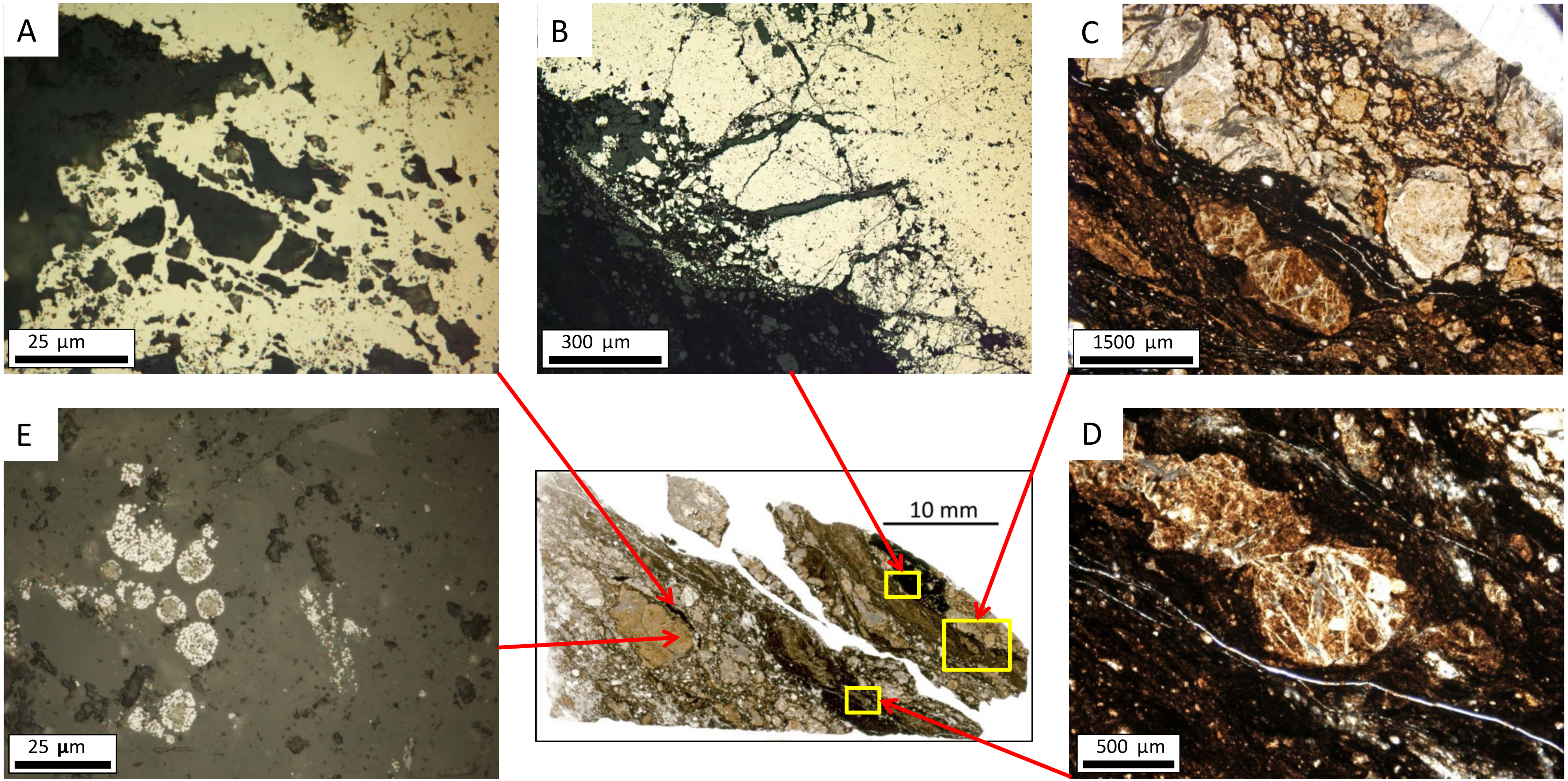

Figure 1. Optical photomicrographs of features in SAFOD specimen thin section G24a. A – RL image of late pyrite filling space between fractured shale fragments. B – RL image of brittle fracturing of polycrystalline pyrite mass. C & D – PPL images of typical gouge with broken shale and siltstone fragments. E – RL image of pyrite framboids in shale fragment.

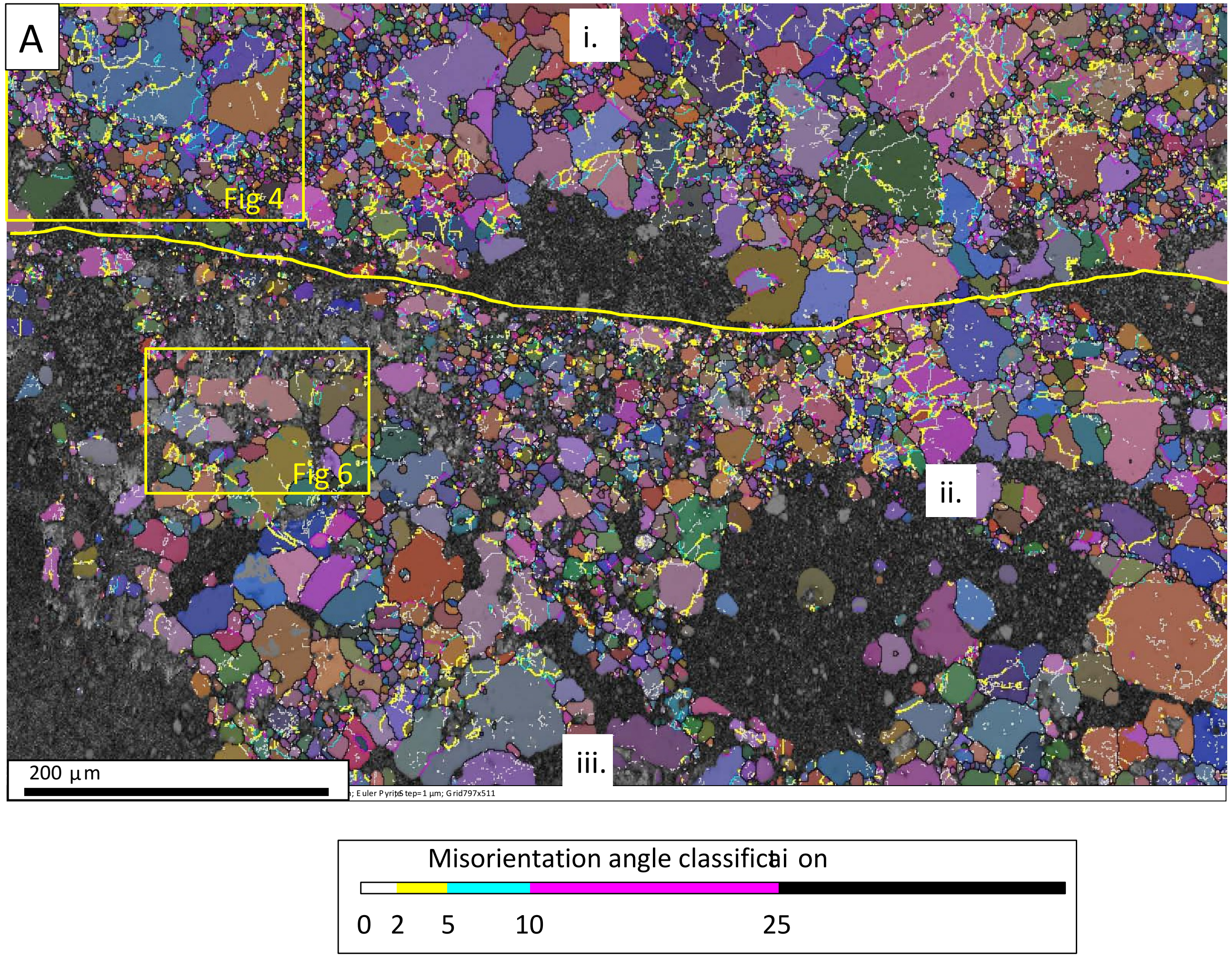

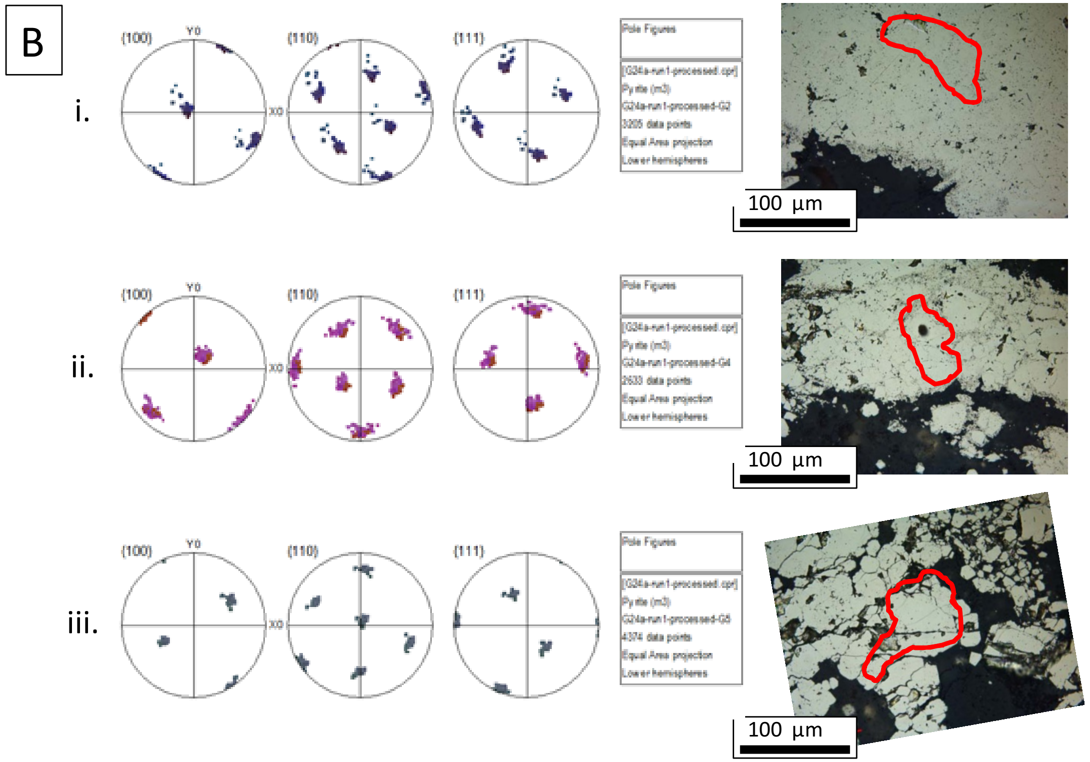

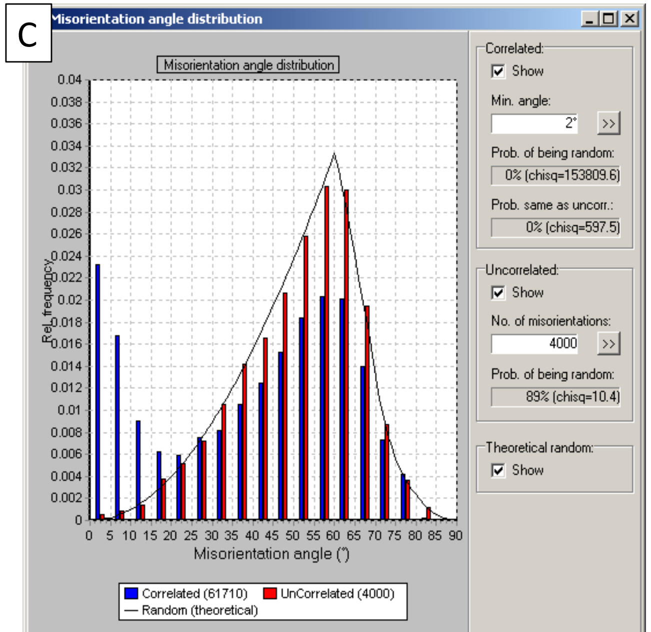

Figure 3. A – 1.0 micron step-size, Euler angle map of pyrite aggregate in polished section G24a. Dif erent colour areas indicate different crystallographic orientat ons. Diff erent colour lines represent vari ions in lattice misorientation ac ross boundaries idenfied in the map. No te the large number of low angle mi - orientation boundaries indicated by the yellow and white lines. The irregular yellow line marks the locc-tion of a shear surface separatng pyrite largely unaf ected by later brittle deformaion (e .g. Figure 4) from pyrite affected by later brittle deformaion (e .g. Figure 6)

B - The three sets of pole figures (i, ii & iii) record evidence for plastc strains (dispersion of data) within individual pyrite grains (outlined in RL images) consistent with dislocation creep.

C - The misorientation angle distribution histogram summarises the development of greater than expec -

Mortar texture indicative of pyrite deformation by subgrain recrystallization (SGR)

- Previous studies of naturally deformed pyrite suggest >400 °C for SGR

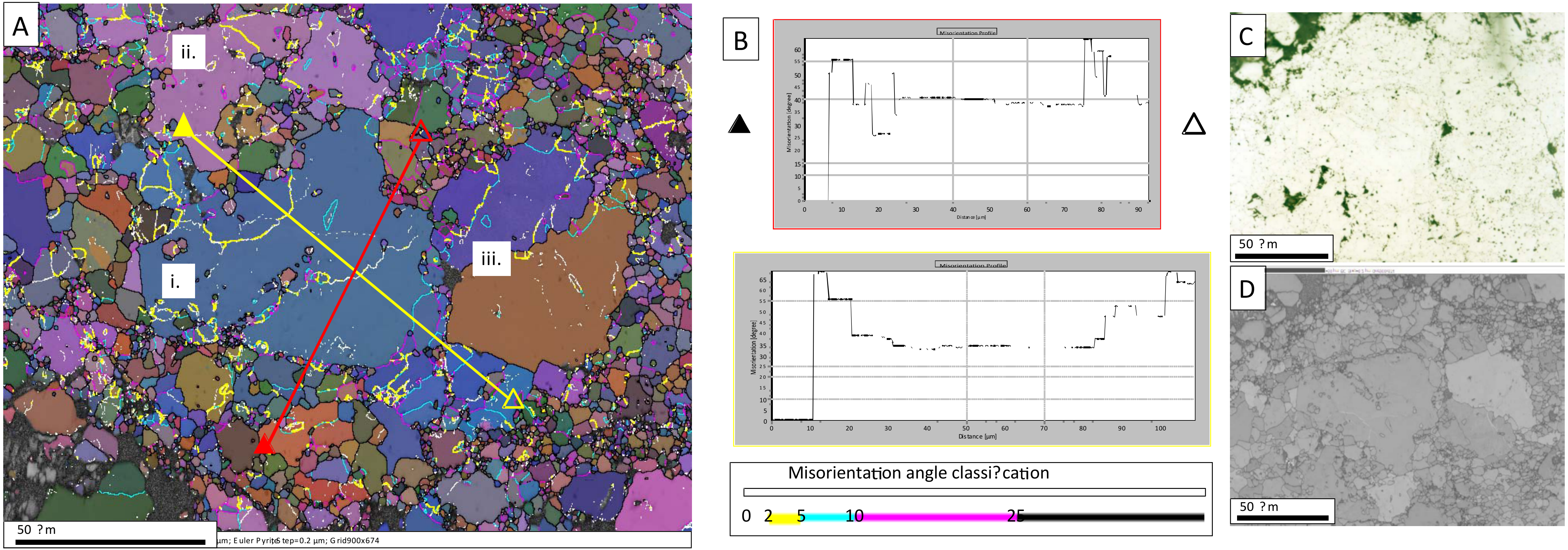

Where does the high temperature come from?

- Inherited from protolith?
- Vertical movements of rocks within the SAF?
- Localised heating from earthquakes?

- Work in progress…

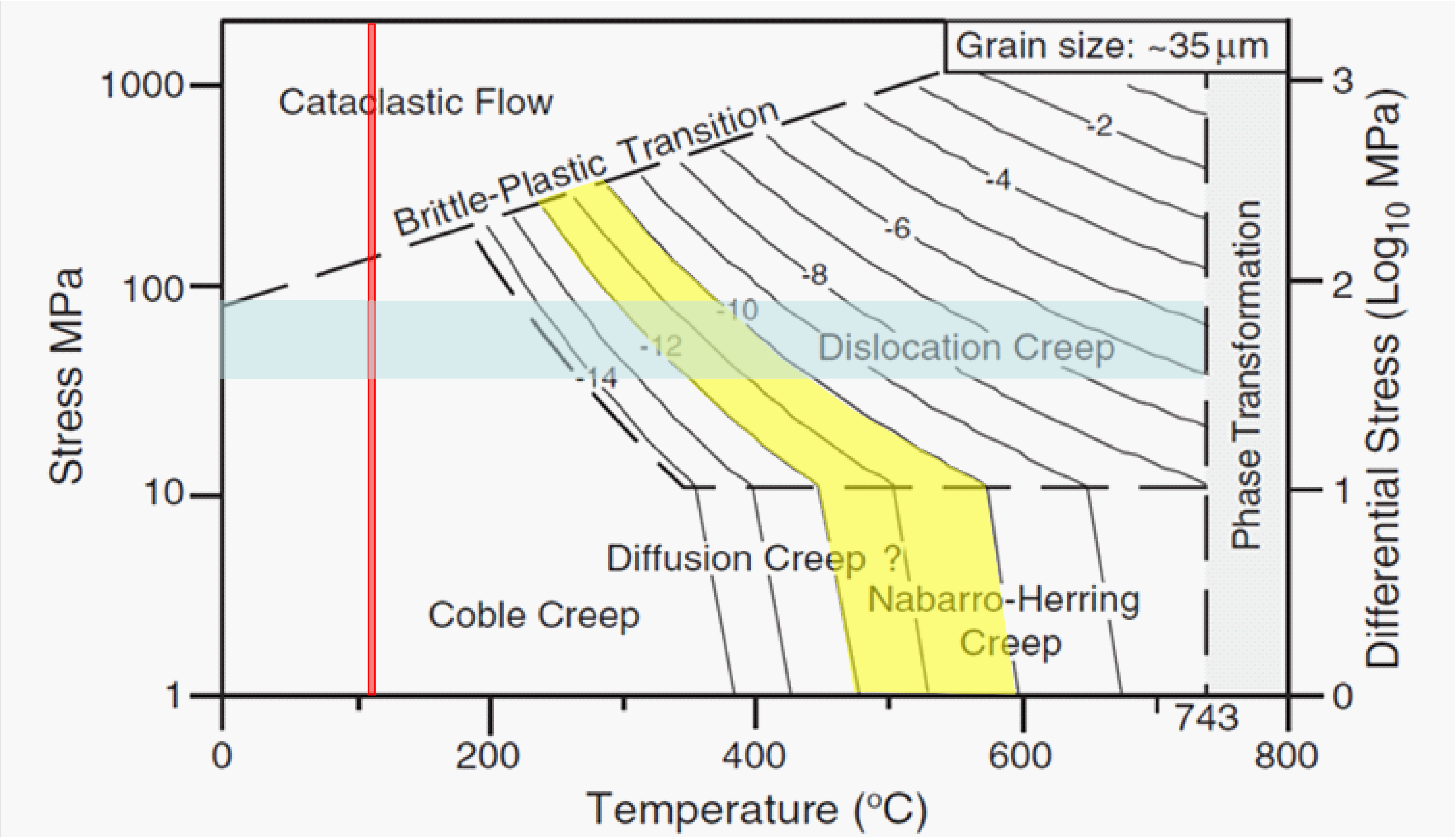

Figure 2. Revised deformation mechanism map from Barrie et al. (2011) for polycrystalline pyrite. The contours on the map are strain rate in units of 10^{-n} s^{-1} and were calculated using experimental stress–strain curves, some of which were presented in Cox et al. (1981). Stress estimates (pale blue band) are from Lockner et al. (2011), strain rate (yellow band) and temperature (red band) estimates are from SAFOD.

Future Directions?

Combine EBSD and Chemistry

Contrib Mineral Petrol (2013) 166:1269–1284
DOI 10.1007/s00410-013-0925-y

ORIGINAL PAPER

Microstructural evolution and trace element mobility in Witwatersrand pyrite

Steven M. Reddy · Robert M. Hough

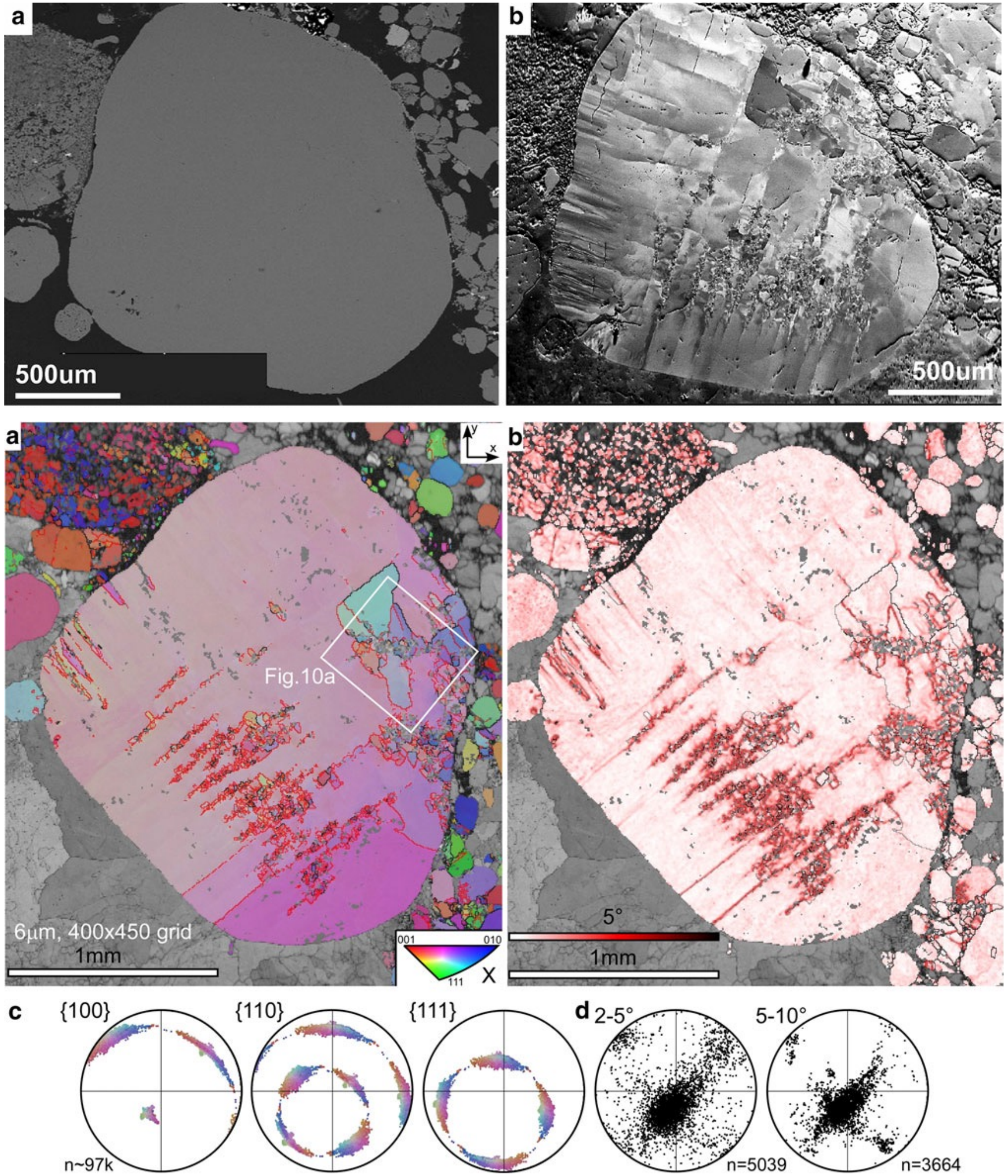

"The data presented here indicate the possibility of gold mobilization and redistribution prior to Central Rand Group deposition by enhanced diffusion of these elements from the matrix into the pyrite along specific low-angle boundaries that behaved as fast-diffusion pathways during an early, high-temperature (>500 °C) deformation event."

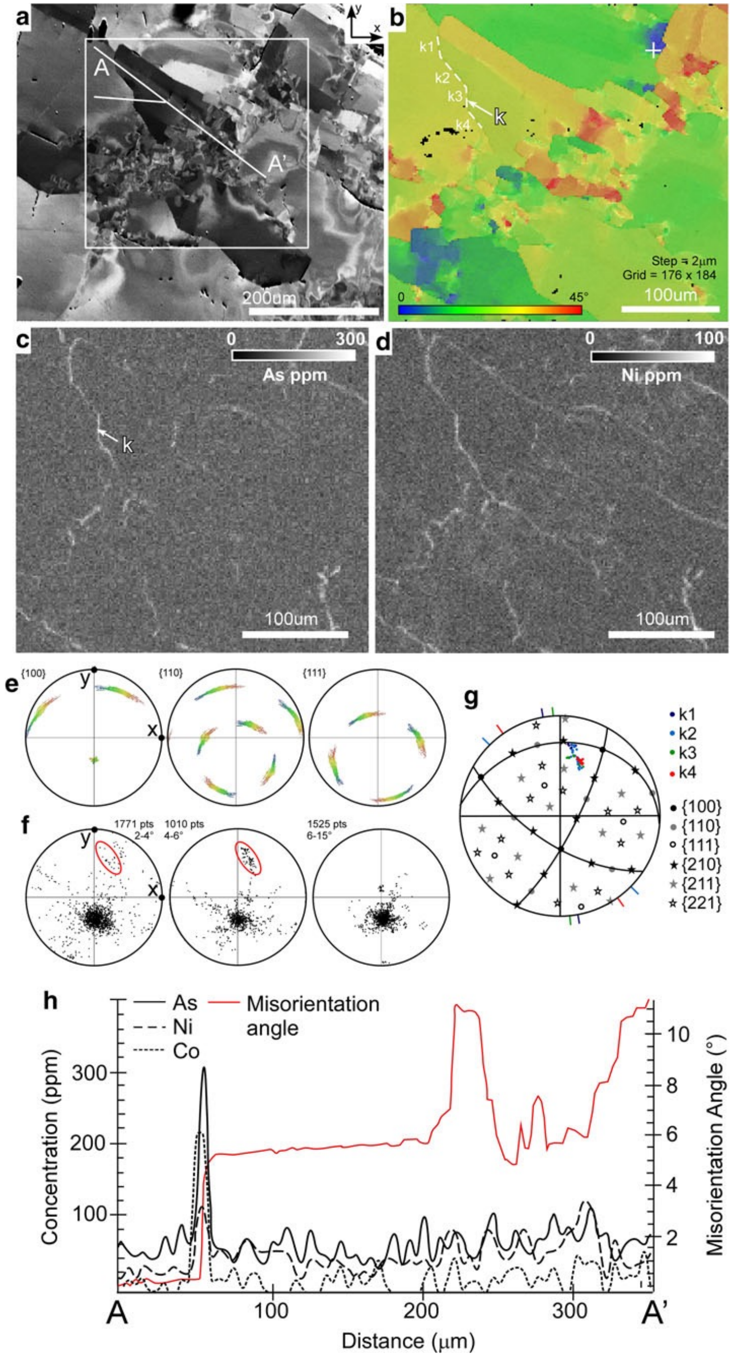

Terra Nova

doi: 10.1111/ter.12206

The golden ark: arsenopyrite crystal plasticity and the retention of gold through high strain and metamorphism

Denis Fougerouse,[1,2] Steven Micklethwaite,[2,3] Angela Halfpenny,[4,5] Steven M. Reddy,[1] John B. Cliff,[6] Laure A. J. Martin,[6] Matt Kilburn,[6] Paul Guagliardo[6] and Stanislav Ulrich[7]

[1]*Department of Applied Geology, Curtin University, GPO Box U1987, Perth, WA 6845, Australia;* [2]*Centre for Exploration Targeting, School of Earth and Environment, The University of Western Australia, M006, 35 Stirling Highway, Crawley, WA 6009, Australia;* [3]*School of Earth, Atmosphere & Environment, Monash University, Melbourne, Vic., Australia;* [4]*Microscopy & Microanalysis Facility, John de Later Centre, Curtin University, GPO BOX U1987, Perth, WA 6845, Australia;* [5]*CSIRO Earth Science and Resource Engineering, Minerals Down Under Flagship, ARRC, 26 Dick Perry Avenue, Kensington, WA 6151, Australia;* [6]*Centre for Microscopy, Characterisation and Analysis, The University of Western Australia, 35 Stirling Highway, Crawley, WA 6009, Australia;* [7]*AngloGold Ashanti Ltd, Asset Development, 44 St George Terrace, Perth, WA 6000, Australia*

Invisible to visible gold?

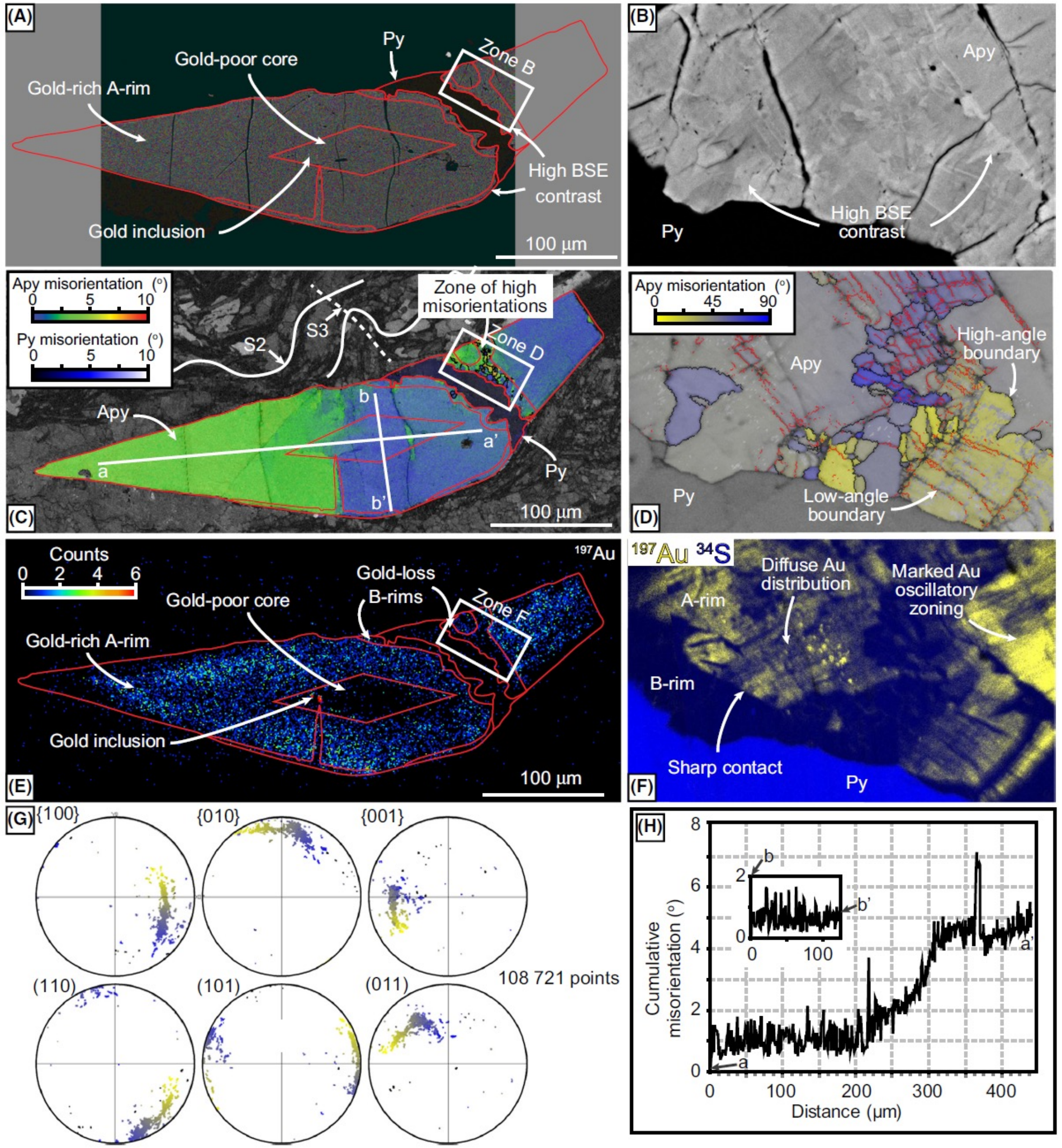

Fig. 3 Sample 215-20, grain 2 – the arsenopyrite boundaries, cores and rims are highlighted in red. (A and B) Backscattered electron (BSE) images. (C and D) Coloured EBSD maps showing crystallographic misorientations in the range 0–10° for (C) and 0–90° for (D). Grain 2 coincides with a crenulation microfold and is weakly deformed by this later overprinting low strain event ($D3_{Ob}$), especially in zone D. High-angle boundaries (≥10°) are plotted in black and low-angle boundaries (≥2°) in red. Dynamic recrystallisation has produced subgrains and new grains. Positions of orientation profiles a–a′ and b–b′ are indicated. (E) SIMS elemental map of ^{197}Au. (F) NanoSIMS composite image of ^{197}Au (yellow) and ^{34}S (blue) elemental distributions. B-rims are gold depleted in comparison to A-rims, and are well developed around zone F. (G) Pole figures show the dispersion of orientation data. (H) Cumulative orientation profiles (plotted relative to first point) parallel to the long axis (a–a′) and short axis (b–b′) of grain 2. The largest crystallographic misorientations are recorded along the crystal long axis (a–a′), parallel to the D3 shortening direction.

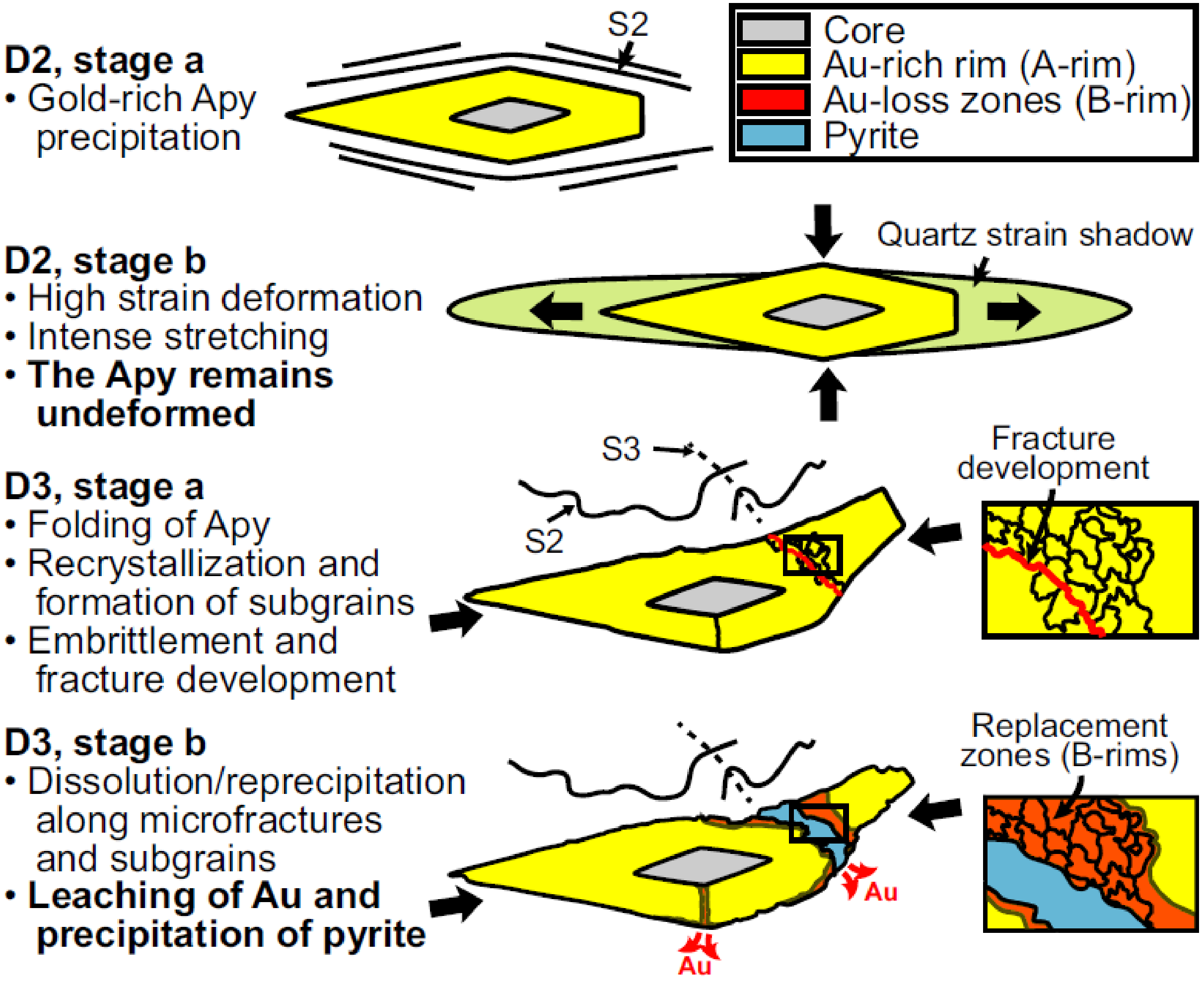

Fig. 4 Interpretation of the microstructural deformation sequence and replacement of arsenopyrite grain 2.

Summary

- Full understanding of microstructure is essential for understanding mineral growth processes, mineral deformation processes, mineral recrystallisation processes, element mobility processes and so on…

- Microstructure should not be investigated without recourse to EBSD

- Studies combining EBSD and microchemistry will become increasingly important

- Time for a short epilogue?

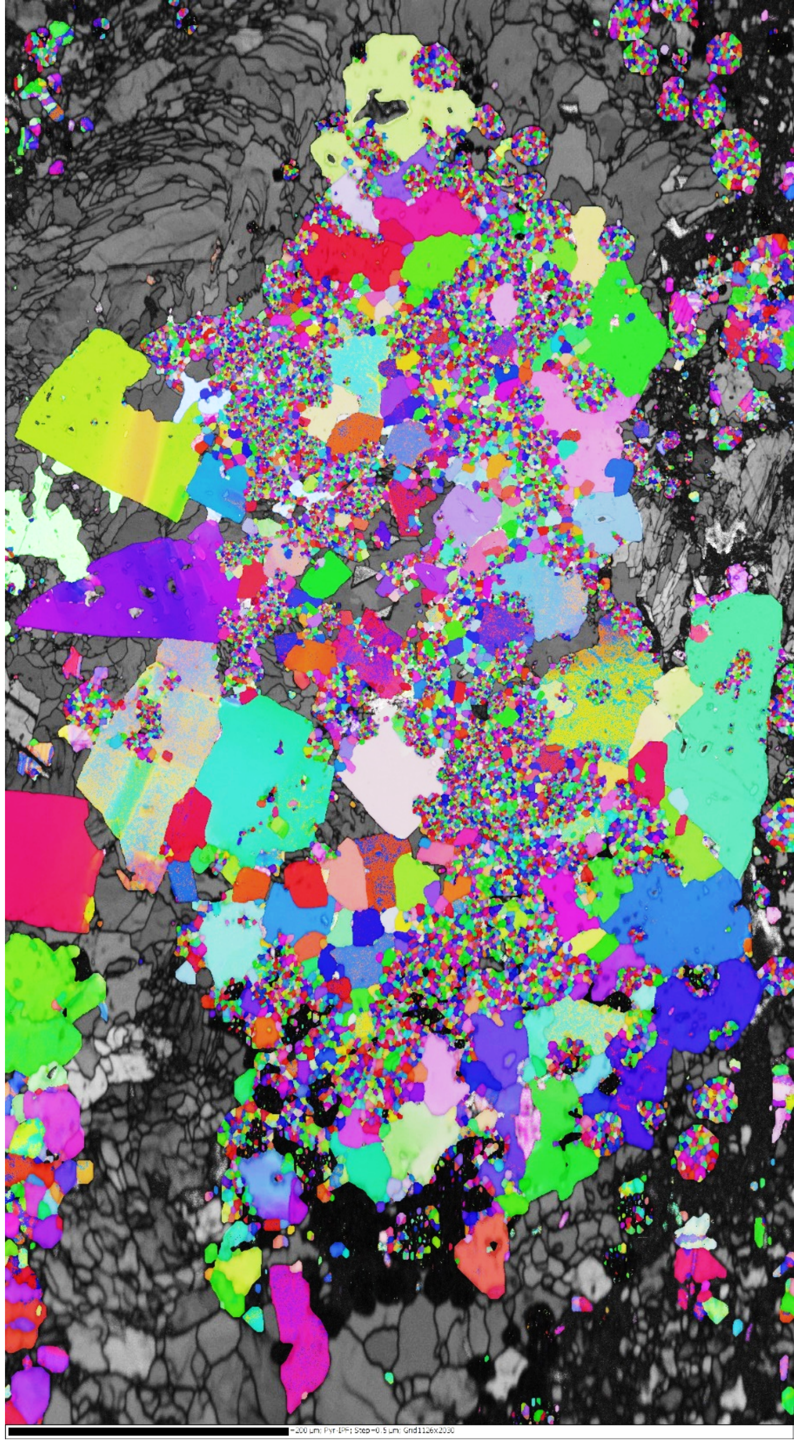

Economic Geology, v. 109, pp. 457–486

Formation and Deformation of Pyrite and Implications for Gold Mineralization in the El Callao District, Venezuela

German Velásquez,[1,2] Didier Béziat,[2] Stefano Salvi,[2,†] Luc Siebenaller,[2] Anastassia Y. Borisova,[2,3] Gleb S. Pokrovski,[2] and Philippe de Parseval[2]

[1] *Universidad Central de Venezuela, Instituto de Ciencias de la Tierra, Avenida Los Ilustres, Los Chaguaramos, Caracas 3895, Venezuela*

[2] *Université de Toulouse, CNRS, Géosciences Environnement Toulouse, Institut de Recherche pour le Développement, Observatoire Midi-Pyrénées, 14 Av. Edouard Belin, F-31400 Toulouse, France*

[3] *Geological Department, Moscow State University, Vorobevu Gory, 119899, Moscow, Russia*

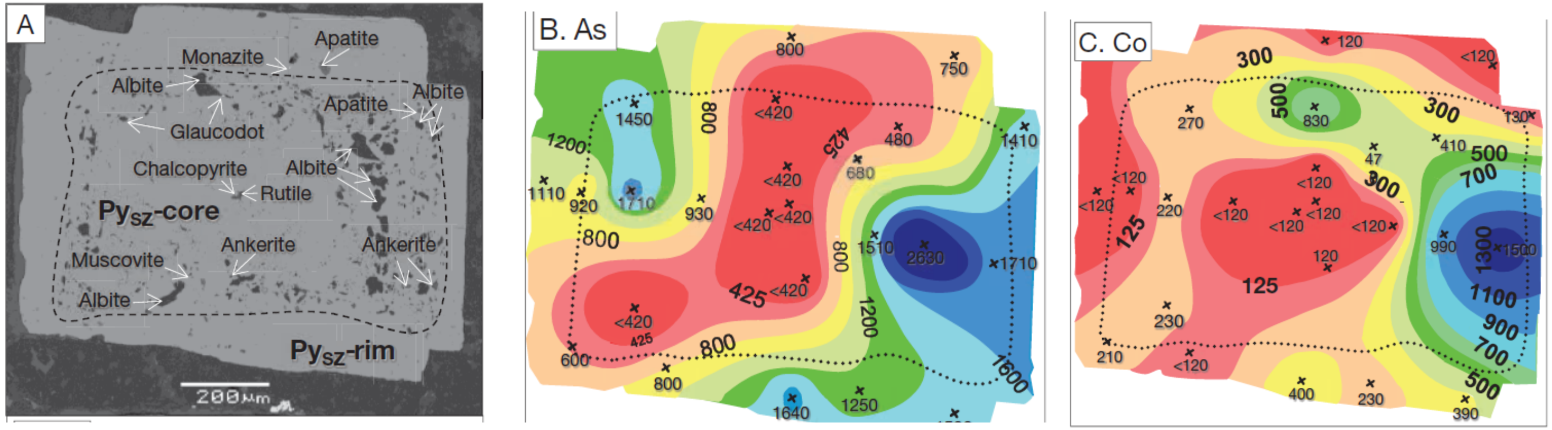
A
Monazite
Apatite
Albite
Apatite
Albite
Glaucodot
Chalcopyrite
Albite
Rutile
Py_{SZ}-core
Muscovite
Ankerite
Ankerite
Albite
Py_{SZ}-rim
200μm
B. As
800
750
1450
800
<420
425
480
1200
680
1410
1110
920
1710
930
<420
<420
<420
800
1510
2630
1710
800
425
<420
1200
<420
425
800
600
1500
800
1640
1250
C. Co
120
300
<120
500
830
300
130
270
47
410
500
700
<120
220
<120
<120
<120
<120
<120
300
125
990
1300
1500
125
120
1100
230
900
700
210
<120
400
230
500
390

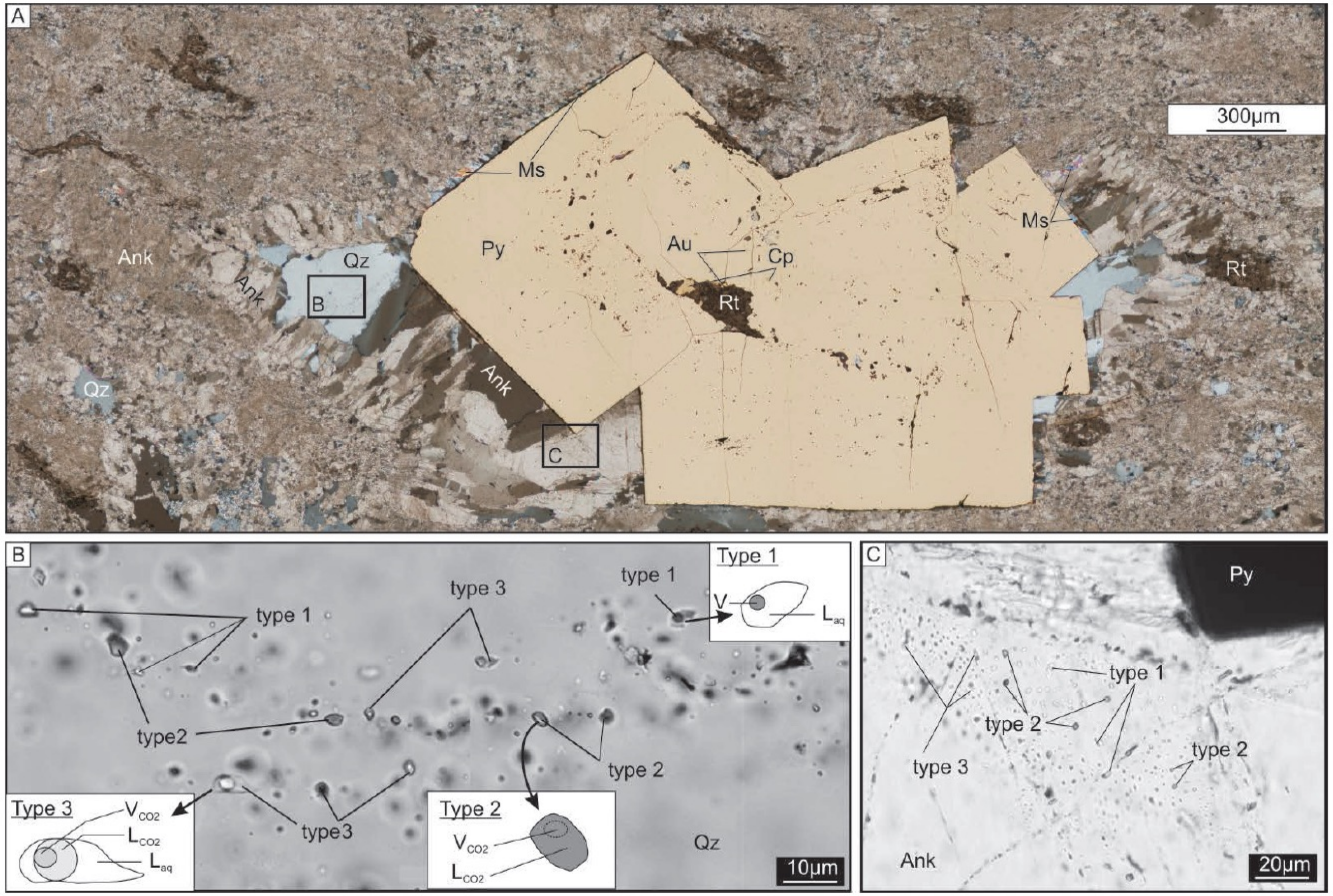
A
300μm
Ms
Ms
Py
Au
Cp
Qz
Ank
Ank
B
Rt
Rt
Qz
Ank
C
B
type 1
type 3
type 1
Type 1
V
L_{aq}
type2
type 2
Type 3
V_{CO2}
L_{CO2}
L_{aq}
type3
Type 2
V_{CO2}
L_{CO2}
Qz
10μm
C
Py
type 1
type 2
type 3
type 2
Ank
20μm

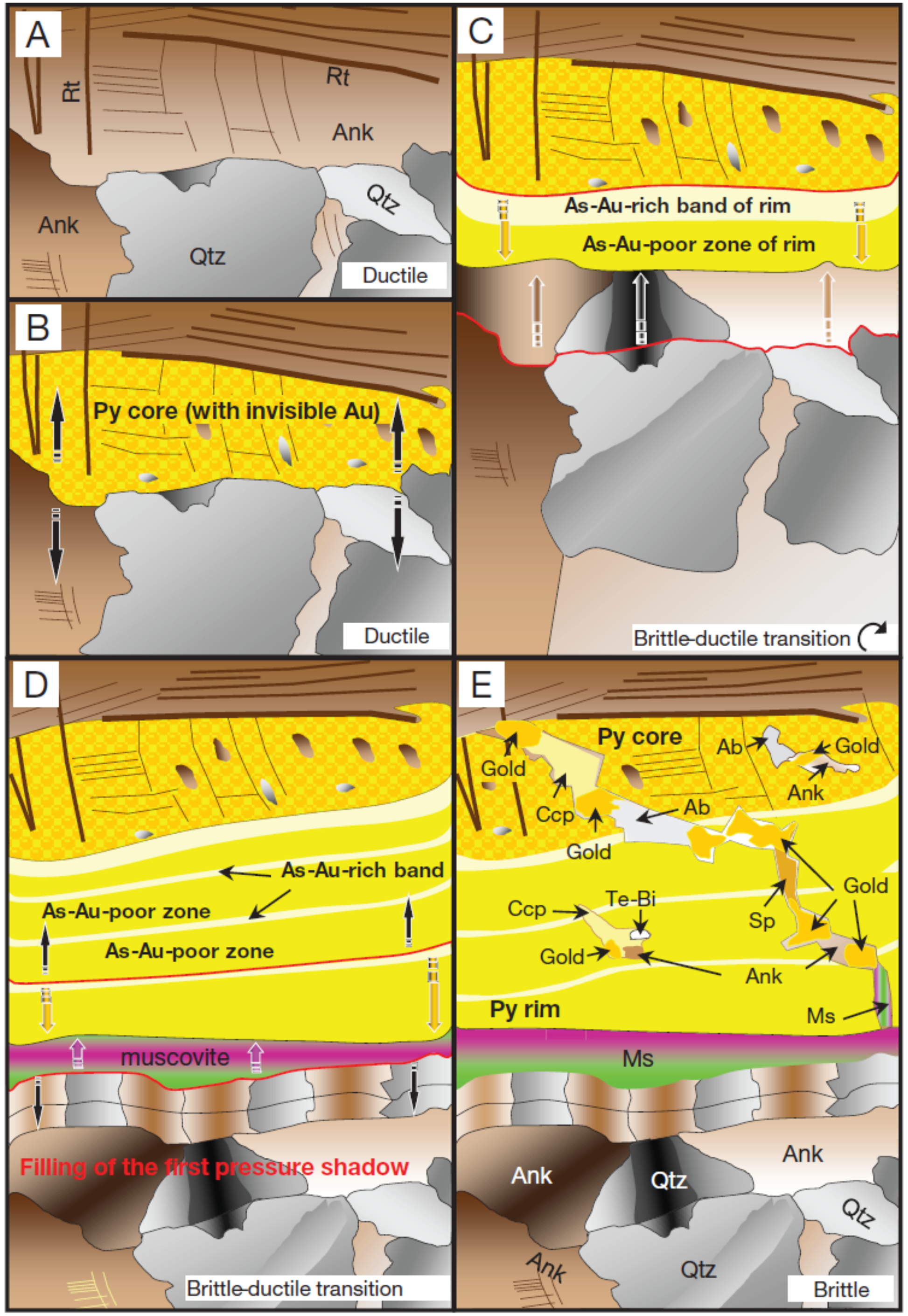
A
Rt
Rt
Ank
Qtz
Ank
Qtz
Ductile
B
Py core (with invisible Au)
Ductile
C
As-Au-rich band of rim
As-Au-poor zone of rim
Brittle-ductile transition
D
As-Au-rich band
As-Au-poor zone
As-Au-poor zone
muscovite
Filling of the first pressure shadow
Brittle-ductile transition
E
Py core
Ab
Gold
Gold
Ank
Ccp
Ab
Gold
Gold
Ccp
Te-Bi
Sp
Gold
Ank
Py rim
Ms
Ms
Ank
Qtz
Ank
Qtz
Ank
Brittle

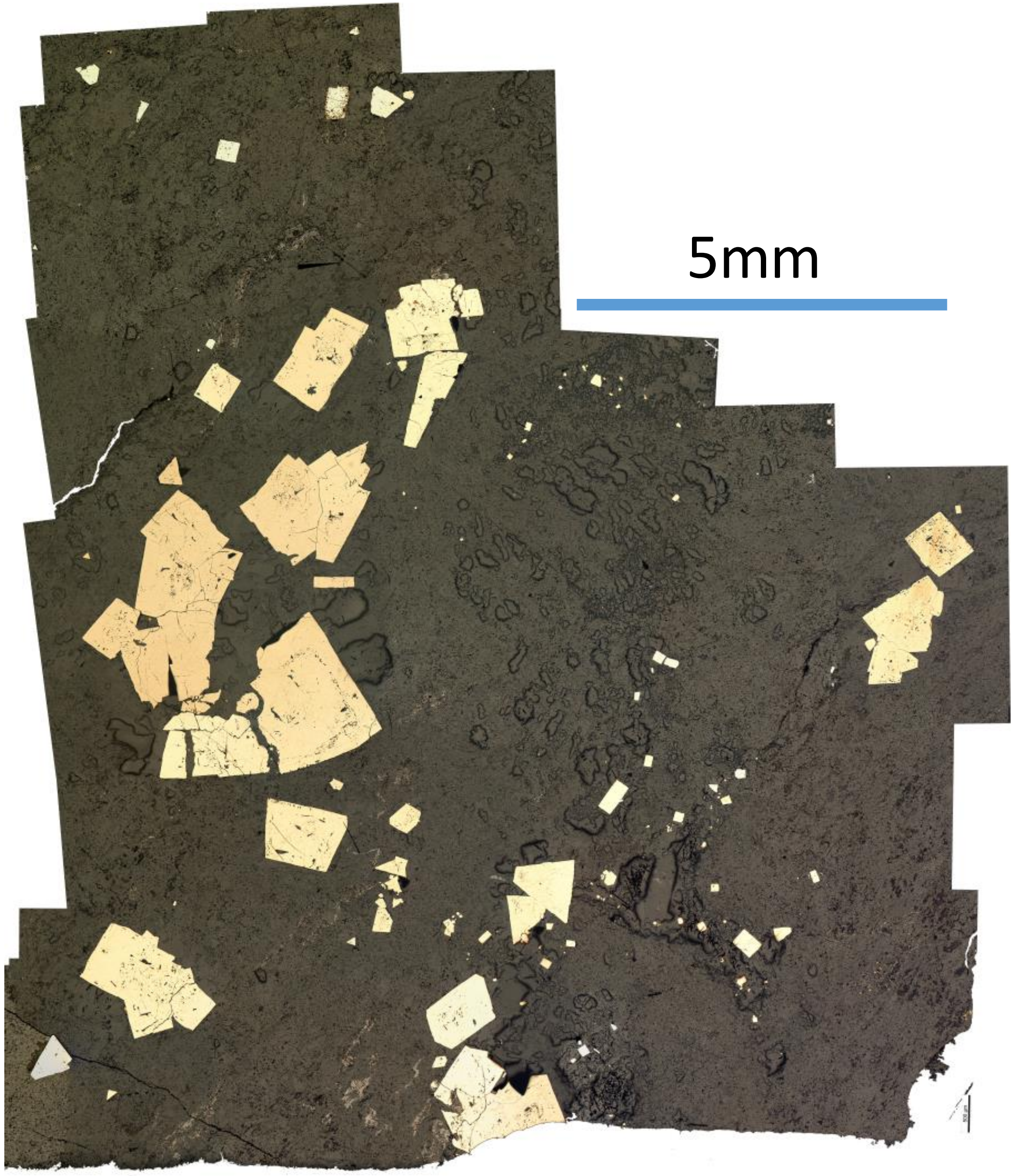

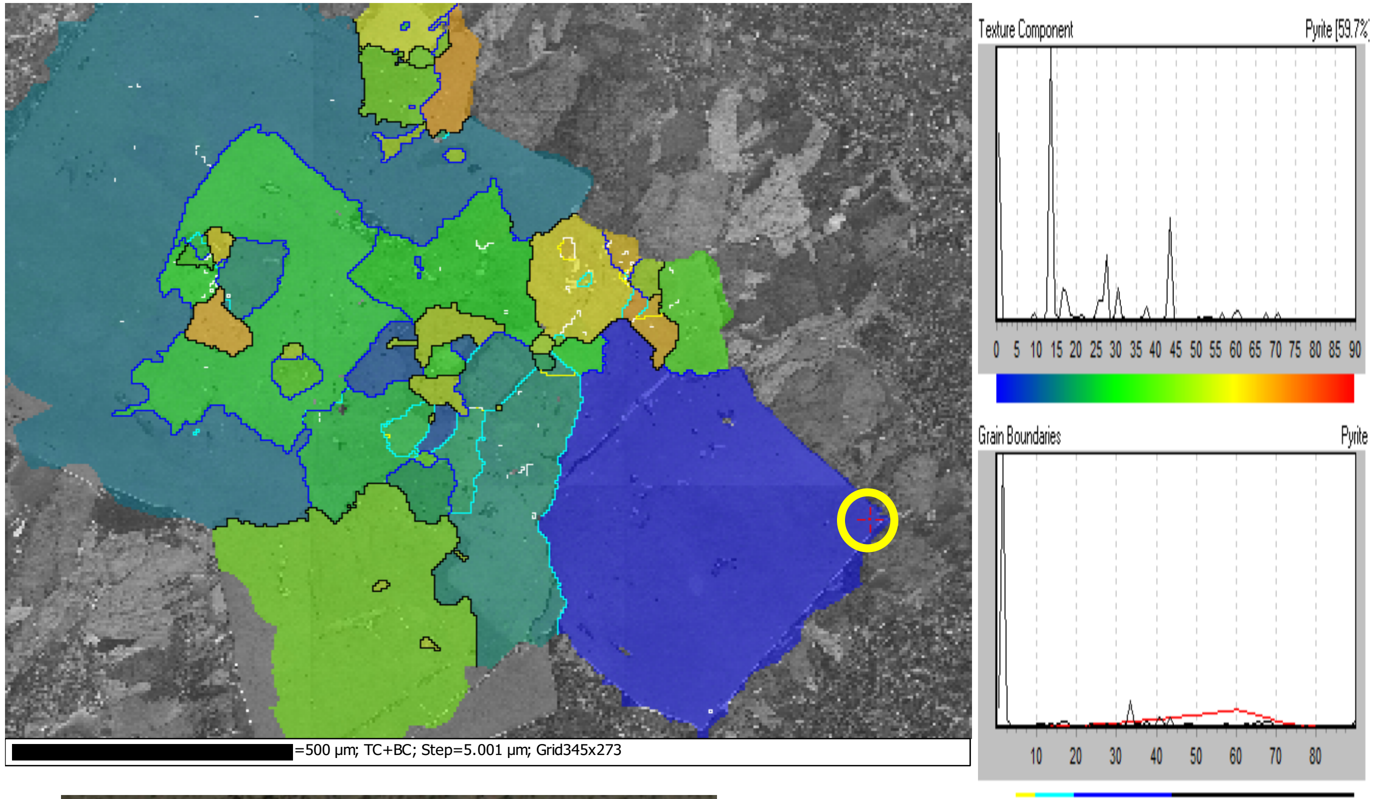

- Texture component map of bottom left pyrite aggregate

- Aggregate comprises deformed and undeformed pyrite grains…
- Misorientation profiles across
  - A – whole aggregate
  - B – Large left side pyrite showing up to 4° internal lattice distortion
  - C – Internal grain showing little or no internal lattice distortion

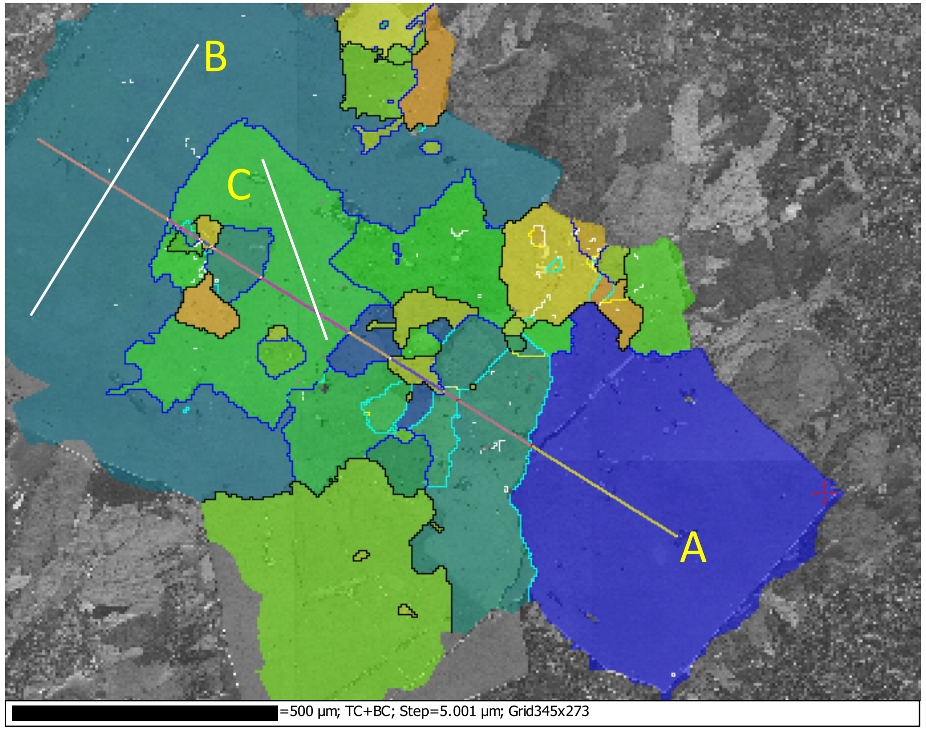

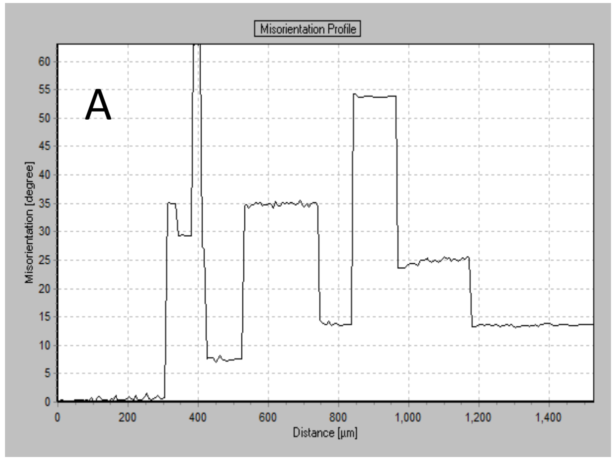

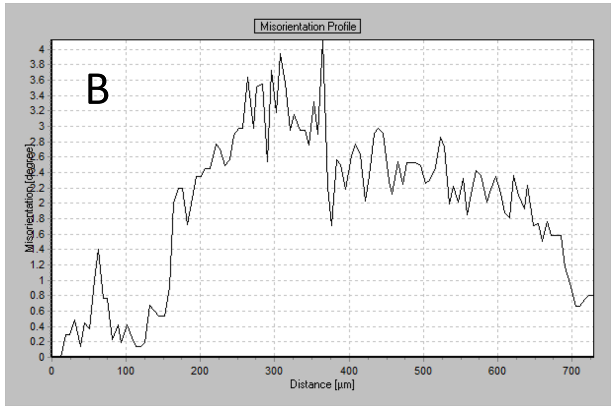

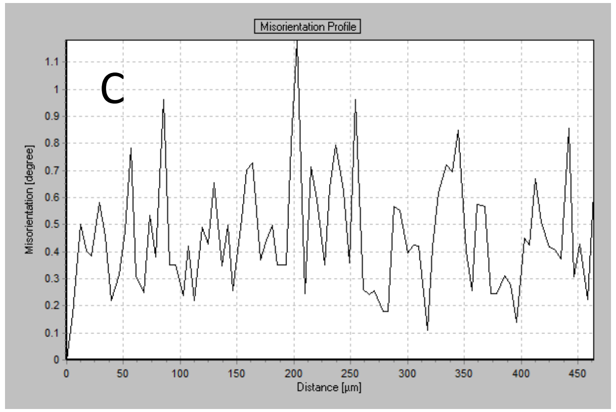

Pole figures for all 70 pyrite grains in the aggregate suggest some weak alignment of grains parallel to <111>.

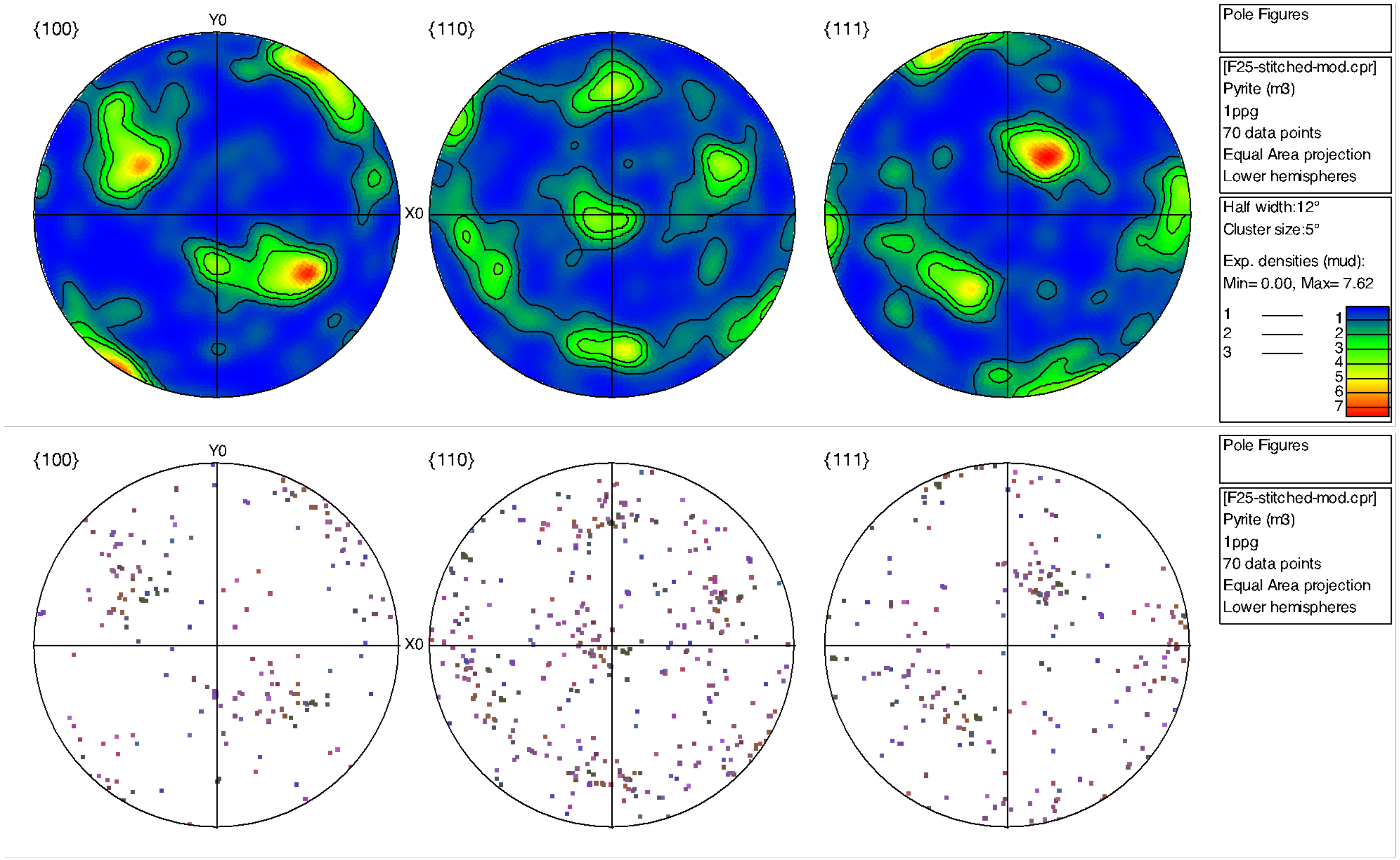

- LH pyrite comprises subgrains with low angle boundaries (white, yellow & cyan) around a polycrystalline core.
- RH aggregate comprises pyrite grains with low angle boundaries and continuous lattice distortion up to ~8°
- Pyrite grains have common {100} direction